FISEVIER

Contents lists available at ScienceDirect

Quaternary Science Reviews

journal homepage: www.elsevier.com/locate/quascirev



The last two glacial cycles in central Patagonia: A precise record from the Nirehuao glacier lobe



Carly Peltier ^{a, b, c, *}, Michael R. Kaplan ^b, Esteban A. Sagredo ^{d, e, f}, Patricio I. Moreno ^{g, e}, José Araos ^h, Sean D. Birkel ⁱ, Rodrigo Villa-Martínez ^{e, f, j, k}, Roseanne Schwartz ^b, Scott A. Reynhout ¹, Joerg M. Schaefer ^{a, b}

- ^a Department of Earth and Environmental Sciences, Columbia University, New York, NY, 10027, USA
- ^b Lamont-Doherty Earth Observatory, Palisades, NY, 10964, USA
- ^c Department of Earth Sciences, Dartmouth College, Hanover, NH, 03755, USA
- ^d Instituto de Geografía, Pontificia Universidad Católica de Chile, Santiago, Chile
- ^e Millennium Nucleus Paleoclimate, Millennium Science Initiative, Santiago, Chile
- f Estación Patagonia de Investigaciones Interdisciplinarias UC, Pontificia Universidad Católica de Chile, Santiago, Chile
- g Institute of Ecology and Biodiversity, Department of Ecological Sciences, Universidad de Chile, Santiago, Chile
- ^h Departamento de Geografía, Facultad de Cs. Sociales, Universidad Alberto Hurtado, Cienfuegos 41, Santiago, Chile
- ⁱ Climate Change Institute & School of Earth and Climate Sciences, University of Maine, Orono, ME, 04469, USA
- ^j Centro de Investigación GAIA-Antártica, Universidad de Magallanes, Punta Arenas, Chile
- k Centro Internacional Cabo de Hornos, Isla Navarino, Chile
- ¹ Departamento de Geología, Facultad de Ciencias Físicas y Matemáticas, Universidad de Chile, Santiago, Chile

ARTICLE INFO

Article history: Received 21 April 2022 Received in revised form 2 November 2022 Accepted 12 November 2022 Available online 15 February 2023

Handling Editor: C. O'Cofaigh

Keywords:
Quaternary
Glaciation
Paleoclimatology
South America
Paleo ice sheet modeling
Patagonia
MIS 6
MIS 2
Glacial geomorphology
¹⁰Be exposure Dating

ABSTRACT

Milankovitch orbital parameters control cycles of insolation, a primary pacer of long term changes in climate, but exactly how insolation signals are transmitted around the globe in the climate system is unclear. In order to address the fundamental questions of when and how ice age climates begin and end, how fast glaciers retreated during the last deglaciation, and how glaciers behaved before anthropogenic influence, we need robust glacial chronologies. The timing of local glacial maxima beyond the last glacial cycle, however, has remained largely unconstrained due to moraine degradation over time, limiting our ability to fully explore these questions. By developing a detailed geomorphic surficial map and targeting relatively tall, ridge-top boulders, we have constructed a new, precise ¹⁰Be chronology of glacial maxima of the Nirehuao glacier lobe (45°S) for the last two glacial cycles. We report one of the first directly dated records of a MIS 6 glacier advance in Patagonia, which formed a major set of moraines by at least 153 \pm 5.1 ka, with a stillstand or smaller readvance by 137 \pm 4.2 ka, corresponding to the two coldest and dustiest periods of MIS 6 in Antarctica. The next largest advance occurred at 23.6 ± 0.9 ka, at the end of peak Southern Hemisphere MIS 2 cooling. Retreat of the glacier commenced by ~18.5 cal ka BP when lakes in a tributary valley just to the southwest became ice-free. Overall we find that advances of the Ñirehuao glacier lobe occur when winter sea ice around Antarctica is expansive and both obliquity and eccentricity are at their minima.

 $\ensuremath{\text{@}}$ 2022 Published by Elsevier Ltd.

1. Introduction

While the dominant periodicity of Northern Hemisphere glaciation during the late Pleistocene is well established as following a

E-mail address: Carly.S.Peltier@Dartmouth.edu (C. Peltier).

~100 kyr cycle (e.g. Hays et al., 1976; Lisiecki and Raymo, 2005; Abe-Ouchi et al., 2013; Roe, 2006), smaller glaciers may not have necessarily followed the same cycle. For example, research in High Mountain Asia has shown that the primary periodicity of glaciation in the region may be dominated by the 23 kyr precession cycle (Yan et al., 2021), and Doughty et al. (2021) suggested that the 41 kyr obliquity cycle may still be an important influence on the timing of glacier advances in many parts of the globe. Testing the global periodicity of ice ages is important for understanding Earth's

^{*} Corresponding author. Department of Earth Sciences, Dartmouth College, Hanover, NH, 03755, USA.

climate system, and requires an interhemispheric array of glacier chronologies on land that extend beyond the last glacial cycle (i.e. the period between the penultimate and the current interglacial periods, or the last ~120 kyr; e.g. Hughes et al., 2013). Marine sediment records provide excellent but indirect estimates of glaciation, and it is a necessity to have independent and direct chronologies on land to test the periodicity of glacier cycles.

In general, relatively little is known about the pre-MIS 2 (29–14 ka; all references to the timing of marine isotope stages are from Lisiecki and Raymo, 2005) glacier advances from terrestrial records world-wide due to the challenges of dating advances this old, which makes it difficult to test the explanatory power of hypotheses on the timing of glacial cycles (e.g., Doughty et al., 2021; Imbrie et al., 1992; Roe, 2006). Patagonia is an ideal region to explore these problems given it has one of the most extensive and well-preserved moraine records on Earth (e.g. Rabassa and Clapperton, 1990; Coronato et al., 2004). The well-preserved glacial deposits in Patagonia offer a unique opportunity to reconstruct glacier and climate history of the region going back multiple glacial cycles.

During glacial periods the Patagonian Ice Sheet covered the southern Andes and flowed out onto the expansive Andean foreland basins on the east side of the Andes, allowing for excellent preservation of glacial features deposited by these outlet lobes. Detailed geomorphic mapping of these deposits has provided valuable insights into glacier-climate dynamics and history, forming the foundation for precise glacier-climate chronologies in the region (e.g., Mendelová et al., 2020; Leger et al., 2021; also see references in Davies et al., 2020), refined understanding of paleoglacier dynamics (e.g. Darvill et al., 2017), and of deglacial lake dynamics and drainage and their impact on local or regional climate (Glasser et al., 2016; Thorndycraft et al., 2019; Vásquez et al., 2022).

While Patagonian studies east of the Andean divide have long recognized nested sequences of moraines outboard of the MIS 2 margin (e.g. Caldenius, 1932; Clapperton, 1993; Mercer, 1976), constraining their absolute timing is challenging. Glacier margins deposited during MIS 2 have been dated using the ¹⁰Be or ¹⁴C methods (see references in Davies et al., 2020), and the outermost as the greatest Patagonian glaciation (GPG) at ~1.1 Ma based on ⁴⁰Ar/³⁹Ar dating of magma flows interbedded with glacial tills (e.g. Mercer, 1976; Singer et al., 2004; Ton-That et al., 1999). The numerous glacial moraines and related landforms between these two time periods remain largely undated in many areas; therefore, the glacier/climate history of this time frame remains elusive. Surface exposure dating of pre-MIS 2 glacier margins has been challenging because positive relief and sloping landforms composed of glacial debris, like moraines and channel walls, tend to diffuse over long timescales, exposing rock surfaces that were shielded upon deposition (e.g. Hein et al., 2009; Heyman et al., 2011, 2016). Recently, a few strategies have emerged that have successfully yielded well-dated pre-MIS 3 (57-29 ka) glacial chronologies in Patagonia. First, targeting landforms created during glacial maxima but that have low relief and low slope angles, like outwash plains and terraces, has led to well-constrained chronologies of glacial maxima back to the GPG (e.g. Hein et al., 2009; Hein et al., 2017, 2011; Darvill et al., 2015; Cogez et al., 2018; Mendelová et al., 2020). Secondly, recent dating efforts informed by detailed geomorphological studies to target well-preserved, tall, ridge-top moraine boulders in a few places around the world have yielded well constrained MIS 4 (71-57 ka) chronologies (e.g. Schaefer et al., 2015; Tulenko et al., 2018; Peltier et al., 2021).

Moraine ridge-top sampling has yet to unequivocally date advances beyond MIS 4 in Patagonia. The recent success of the method in southern Patagonia in dating MIS 4 moraines (Peltier

et al., 2021), earlier efforts in central Patagonia (Kaplan et al., 2005; Hein et al., 2017), and statistical and landform modeling studies more broadly (Putkonen and Swanson, 2003; Applegate et al., 2010; Heyman et al., 2011, 2016) highlight the strategies that allow us to overcome the issue of moraine denudation. First. targeting boulders taller than at least a meter may be important for older moraines. By dating multiple boulders on the same landform. Peltier et al. (2021) showed that boulders below about a meter in height may be more likely to yield younger ages (cf., Kaplan et al., 2005), even for boulders on the center of moraine crests. Second, pairing chronological work with detailed geomorphic study helps inform the sampling strategy to target moraines with better preserved surfaces (e.g., Sagredo et al., 2011; García et al., 2014; Robb et al., 2015; Mendelová et al., 2020; Leger et al., 2021, among many others, including those referenced in Davies et al., 2020). We apply these strategies to the moraines deposited by the Nirehuao glacier lobe (Fig. 1) to produce the first chronologic constraints of glacier advances that led to their formation, and one of the first successful applications of the moraine boulder dating technique to moraines deposited before the last glacial cycle in Patagonia.

Furthermore, the timing, structure, and magnitude of the last glacial maximum (LGM; ~26-19 ka, Clark et al., 2009) and its possible latitude-dependence is an important and outstanding problem in our understanding of glacial cycles in Patagonia. The LGM provides an important constraint on the sensitivity of Earth's climate system (e.g. Schmittner et al., 2011; Tierney et al., 2020). Existing glacial chronologies from southern Patagonia suggest that glaciers culminated multiple times during the LGM, and were most extensive towards the beginning of MIS 2 (~27-25 ka), and again towards the end (~23-18 ka) (Hein et al., 2010; Darvill et al., 2016; Peltier et al., 2021). This bimodal MIS 2 may be related to variations of the southern mid-latitude atmospheric circulation associated to past changes in the Subantarctic and Antarctic Circumpolar Current systems, as some Antarctic records have a similar bimodal MIS 2 (e.g. Antarctic temperature (Parrenin et al., 2013) and dust flux (Lambert et al., 2012), but this remains untested in central and northern Patagonia.

Here we apply insights from recent, precise, pre-LGM ¹⁰Be exposure dating of moraines to understand the timing, structure and drivers of the MIS 2, MIS 6 (191–130 ka), and pre-MIS 6 advances of the Nirehuao glacier lobe. We also present a detailed geomorphic map with a focus on the terminal deposits of the local LGM and beyond, with the goal of understanding the Nirehuao glacier lobe dynamics and history.

2. Setting and climate

The Río Ñirehuao (also spelled Ñireguao and Ñiregüao) valley (45.2°S, 71.5°W) is located ~60 km northeast of the city of Coyhaique in the Aysén Province of Chile, within the Southern Volcanic Zone near recently active volcanoes (e.g. Cerro Hudson, Macá, Cay, Mentolat), just north of the Patagonian Volcanic Gap (Fig. 1A; e.g. Stern, 2004). The region is located north of the modern position of the core of the Southern Hemisphere Westerly Winds (50–55°S; e.g. Moreno et al., 2018). The area contains a semi-arid climate as it is located on the lee side of the Andes, and it is subject to the subsidence of dry air (Garreaud et al., 2009). Consequently, there is a strong longitudinal precipitation gradient; precipitation declines from ~4200 mm/yr on the Pacific Coast (Isla San Pedro) to ~670 mm/yr in Coyhaique Alto, ~30 m due south of the study site (Hepp et al., 2018).

The Rio Nirehuao basin is bound to the west by the Andes and to the east by a sequence of terminal moraines. The crest of these moraines forms the border between Argentina and Chile, as well as

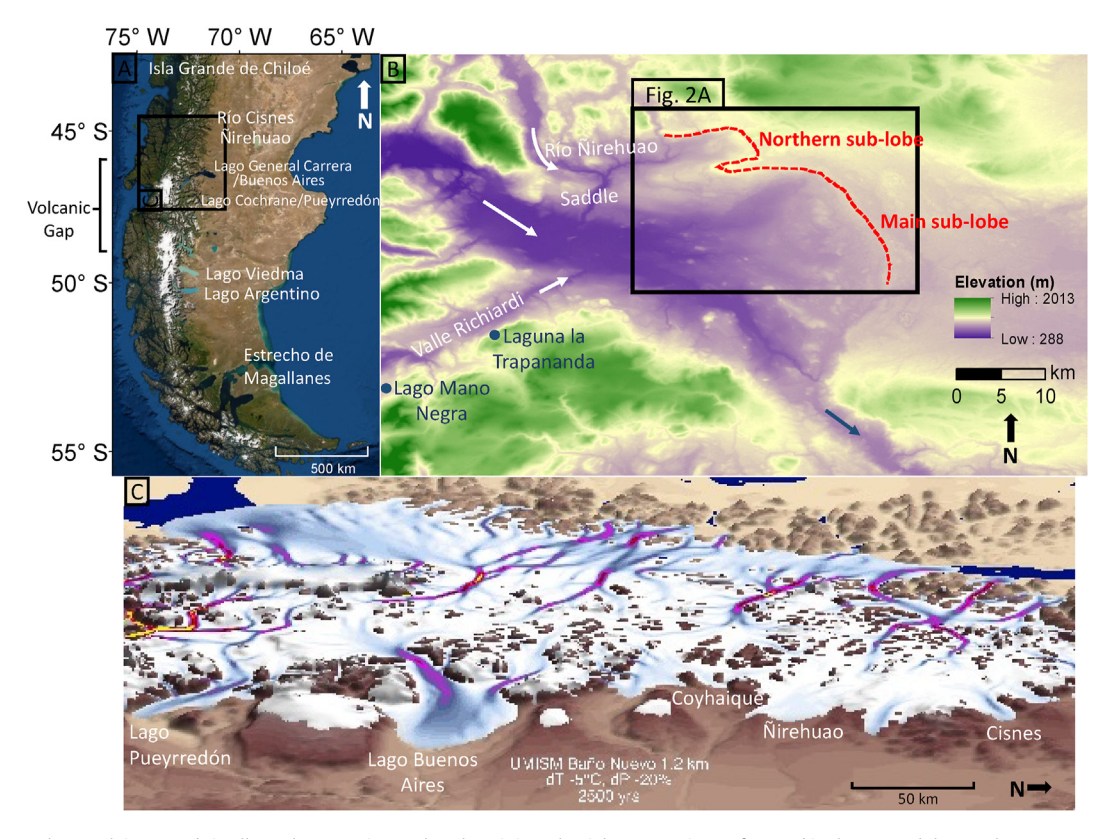


Fig. 1. Study site. Note that north is upwards in all panels, except in Panel C where it is to the right. **A.** Locations referenced in the text and the panel C extent. **B.** ALOS PALSAR digital elevation model of the Río Ñirehuao valley. The red dashed line marks the core of the Ñire 1 moraine complex and outlines the two sub-lobes that terminate within the mapped area which together form what we call the Ñirehuao lobe. The area where the two sub-lobes meet, where the red dashed line follows a "V" shape, is referred to in the text as the interlobe area. White arrows indicate the paleo flow directions of the three main tributary glaciers within the Ñirehuao valley. Blue arrow near the bottom marks the ~750 masl spillway to the Atlantic. **C.** Oblique view of a reconstruction of the central sector of the Patagonian Ice Sheet during the LGM, showing Ñirehuao and neighboring lobes, from the University of Maine Ice Sheet Model (UMISM) with ice velocity rendered on the ice surface (a description of UMISM is available in Peltier et al., 2021). (For interpretation of the references to colour in this figure legend, the reader is referred to the Web version of this article.)

the continental drainage divide, which is well east of the highest summits of the Andes. Río Ñirehuao enters the valley from the north (Fig. 1B) and flows out through the Andes to the west. This study focuses on the glacial deposits left by the Ñirehuao glacier lobe of the Patagonian Ice Sheet that flowed eastward out of the Andes to terminate in the pre-cordillera.

3. Prior work

3.1. Past studies in the area

The earliest glacial geomorphic study in this area was conducted by Caldenius (1932) and has been subsequently mapped as part of efforts to map the terminal landforms of the whole ice sheet (Caldenius, 1932; Davies et al., 2020; Glasser and Jansson, 2008; Glasser et al., 2008). Most recently, Cooper et al. (2021) mapped a section of the terminal landforms of the ice sheet (44°-46°S) including the whole Nirehuao lobe and its neighboring lobes, affording an excellent broad-scale context to our map that focuses on the northern half of the Nirehuao lobe in greater detail. Some outlines of the LGM moraines and a paleolake shoreline were also previously mapped as a means of targeting archeological sites for ground surveys above the paleolake level (Méndez et al., 2019). The neighboring Río Cisnes glacial valley to the north was mapped with the aim of developing a chronology of glacial events (García et al., 2019). Further north, ~200 km north of Nirehuao, Leger et al. (2020) mapped in detail the glacial valleys around Río Corcovado. Lago Buenos Aires, ~150 km south of Nirehuao, has been the focus of multiple mapping and dating efforts (Singer et al., 2004; Kaplan et al., 2004, 2005; Douglass et al., 2006; Smedley et al., 2016; Bendle et al., 2017; Hein et al., 2017; Cogez et al., 2018).

With the exception of a single 14 C basal age from a tributary valley to the Ñirehuao glacier, the Ñirehuao glacier lobe history has remained completely unconstrained in terms of chronology. Laguna La Trapananda (blue dot in Valle Richiardi in Fig. 1B; -45.335° , -71.791°) produced a 14 C basal age of 18.5 ± 0.2 cal ka BP (calendar years before the present, we use this unit for radiocarbon ages following convention) implying that by this time the site at 1160 masl was ice free (Weller et al., 2019).

About 80 km north of the Nirehuao valley, in the Río Cisnes valley (Fig. 1C), García et al. (2019) mapped two undated moraines, CIS I and CIS II, which they assumed to be MIS 2 in age. About 15 km inboard of these moraines, they dated a recessional moraine to 20.1 \pm 1.2 ka and inferred that recession started prior to ~19.0 ka, and by 16.9 \pm 0.3 ka the glacier occupied only ~40% of its full LGM extent.

The Coyhaique glacier lobe just to the south (Fig. 1C) reached its maximum extent multiple times during MIS 2, where the most recent maximum occurred after ~21.8 ka (Miranda, 2015). The glacier retreated and abandoned the innermost LGM margin at ~17.9 cal ka BP (Vilanova et al., 2019; Villa-Martínez and Moreno, 2021). This was followed by the formation of an ice-dammed lake and a stepwise glacier retreat, with a stillstand or readvance at ~16.8 cal ka BP. The lake level reached a highstand of 650—726 masl between ~17.9 and 17.2 cal ka BP and lowered to 570—650 masl between ~17.2 and 16.2 cal ka BP (Vilanova et al., 2019; Villa-

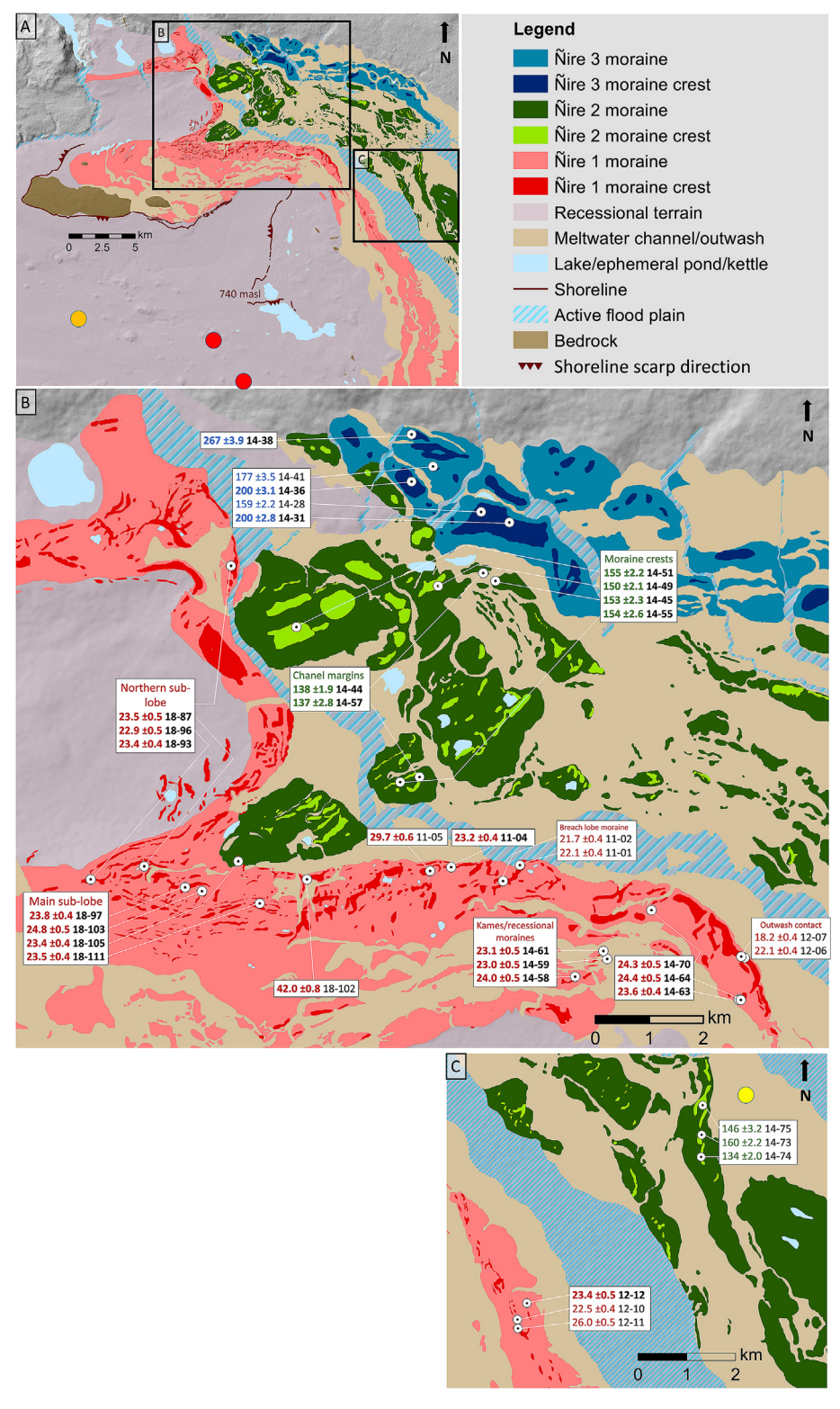


Fig. 2. New geomorphic map and 37 new ¹⁰Be ages. Individual samples are shown with their internal error and sample name in black. Ages in bold are included in the mean ages. The paleo-glacier lobes overall flowed eastward. A. Full mapped extent. Orange dot indicates the location of the tuff cone pictured in Fig. 4. Red dots indicate the locations of the archeological sites, Cueva de la Vieja (northwest dot) and Baño Nuevo 1 (southeast dot). B. Left lateral moraines of the main sub-lobe and the moraines deposited by the northern sub-lobe. The area where the terminal margins of the two sub-lobes meet, where the moraine complex has a "V" shape, is referred to in the text as the interlobe area. C. Frontal moraines and outwash plains of the main sub-lobe. Yellow dot on panel indicates the location of outwash outcrop in Fig. 5. (For interpretation of the references to colour in this figure legend, the reader is referred to the Web version of this article.)

Martínez and Moreno, 2021), after which the glacier lake drained to the Pacific Ocean (Miranda, 2015). Closed basin lakes have provided a look into the paleovegetation and paleoclimate of the area since the last glacial termination, showing an afforestation trend that started at ~16.6 cal ka BP in response to enhanced influence of the southern hemisphere westerly winds at that latitude. This signal followed the disintegration of the Patagonian Ice Sheet in response to warmer conditions throughout western Patagonia starting at ~17.9 cal ka BP, a concomitant poleward shift of the westerlies that lasted until ~16.6 cal ka BP, followed by a subsequent northward shift to its mean interglacial position (Villa-Martínez and Moreno, 2021).

The Ñirehuao valley has been the subject of petrologic work, as the area between the international border and the town of Ñirehuao is spotted by tuff cones (with heights of ~100 m and diameters of 0.5–1.5 km) formed by magmatic eruptions into a shallow sea at ~120 Ma (e.g. Suárez et al., 2010). These tuff cones were subsequently sculpted by Pleistocene glacier advances, and frequently have tails of till on the downflow side (Fig. 4) superimposed by lacustrine deposits (e.g. regressive beach ridges).

The Nirehuao valley is also an important archeological site, as caves in the tuff cones were subject to human occupation. Western Patagonia is suggested to have been one of the last areas to become occupied by humans in the southern cone, in part due to the inhospitable climate of the periglacial region during the last glaciation (Méndez et al., 2018). The caves have yielded human skeletal remains, representing a minimum age for the initial peopling of the area of ~12 cal ka BP (red dots in Fig. 2A; Mena et al., 2003; Méndez et al., 2018). This suggests that the climate in the Nirehuao basin was temperate enough after ~12 ka to allow for viable ecosystems that might attract hunter-gatherers (Méndez et al., 2018).

3.2. Existing direct dating of Patagonian glacier advances prior to the last glacial cycle

Kaplan et al. (2005) dated the Moreno I and Moreno II moraines at Lago Buenos Aires (46.5°S; Fig. 1A and C) and inferred they formed during MIS 6. The ages on both moraines have a large scatter and range (~143-37 and ~150-80 ka), and in some cases are inconsistent with the 40Ar/39Ar dated lava flow (~109 ka) that provides a minimum age of the Moreno moraines (Singer et al., 2004). Smedley et al. (2016) also produced optically stimulated luminescence ages from major proglacial outwash deposits at Lago Buenos Aires that suggest the Moreno moraines formed during the interval between 150 \pm 30 ka and 110 \pm 20 ka. Sugden et al. (2009, 2017) dated cobbles from outwash plains associated with the Moreno moraines at the Lago Buenos Aires and Lago Pueyrredón valleys (47.5°S; Fig. 1A and C) to ~270-260 ka, meaning that the boulder ages may underestimate the true moraine age by ~100 kyr and suggest that they were deposited during MIS 8 (~300–243 ka). Hein et al. (2009, 2017) argued that outwash plains tend to be better preserved than moraine surfaces because of their low angle slopes, while moraines tend to degrade over time. Hence, Hein et al. (2017) inferred at Lago Buenos Aires that the evidence was lacking for a MIS 6 glacial maximum and the ages in Kaplan et al. (2005) should be treated as minimum age estimates. Furthermore, because MIS 2 deposits are the next preserved set of landforms inboard of the ~270-260 ka deposits, any advance that occurred after MIS 8 must have been similar in size, or perhaps smaller, than the MIS 2 advance for the Lago Buenos Aires and the Lago Pueyrredón glacier lobes. To date, the only other studies that have directly dated Patagonian glacial advances prior to the last glacial cycle also focus on the Lago Buenos Aires and the Lago Pueyrredón glacier lobes, documenting glacial advances to MIS 12 and beyond by focusing mainly on outwash deposits (Hein et al., 2011; Cogez et al., 2018; Tobal et al., 2021).

4. Methods

4.1. Geomorphic mapping

We carried out geomorphic mapping using ArcGIS 10.6 software based on remote sensing and field observation. We used GEOTEC aerial photos from the Servicio Aerofotogramétrico de la Fuerza Aérea de Chile (Fig. 3; 1:70.000) with coverage over our entire mapped extent (Fig. 2). We used the original photographs developed from the film strips to maximize the visible detail, and scanned and georeferenced the photos in ArcMap to ESRI™ World Imagery layer (15 m TerraColor and 2.5 m SPOT) to facilitate the translation from the stereoscope view onto the map in ArcGIS. Where the aerial imagery was overexposed we mapped features over ESRI imagery. We also referenced Google Earth imagery and Advance Land Observation Satellite (ALOS PALSAR, ~12 m spatial resolution) digital elevation models. We ground-truthed the mapping work over multiple field visits when we covered the area shown in Fig. 2B, with the exception of the sector heavily dissected by outwash on the farthest east Nire 2 and 3 moraines. We focused on the terminal and left lateral moraines from the local LGM (i.e. the innermost moraine on the east side of the Nirehuao basin) and the two prominent moraine complexes just outboard, and mapped in detail all surficial glacial features present. We map the geomorphic features following well-established Patagonian glacial geomorphic mapping criteria (e.g. Glasser et al., 2008; Darvill et al., 2014; Bendle et al., 2017; Soteres et al., 2020).

We aimed to reduce bias and create a map that is informed by observation (rather than interpretation) by (1) mapping in detail all glacial features present within the study area to develop a geomorphologic scheme devoid of a priori interpretations, and (2) by mapping each individual feature (e.g. kettle, moraine crest) rather than grouping areas into interpreted landform types (e.g. kettle topography, moraine terrane). We aim to make these generalizations and interpretations in the main text rather than on the map.

4.2. Glacial chronology

We sampled moraine boulders for ¹⁰Be surface exposure dating during field campaigns in 2011, 2012, 2014, and 2018 (the first number in each sample name is the year it was collected). We sampled mostly boulders on the tops of moraine crests, but also sampled three boulders (BN-14-44, BN-14-57, BN-14-74) on the slopes of moraine crests where they are cut by meltwater channels in locations where moraine ridge-top boulders were unavailable, in order to date the timing of meltwater channel incision (Fig. 6). We measured the sample locations with a handheld Garmin GPS (WGS84) with a reported accuracy of within 15 m. Boulder heights were measured from the sampled surface to the moraine surface on the tallest side of the boulder (except for BN-14-58, -63 and -74, which we approximated using field photos). We isolated $^{10}\mathrm{Be}$ at the Lamont-Doherty Cosmogenic Nuclide Laboratory using standard methods (e.g., Schaefer et al., 2009; Kaplan et al., 2011) and measured the samples at the Lawrence Livermore National Laboratory Center for Accelerator Mass Spectrometry (Table 1). Ratios were measured relative to the standard 07KNSTD3110, with a 10 Be/ 9 Be ratio of 2.85 \times 10 $^{-12}$ (Nishiizumi et al., 2007). We used version 3 of the CRONUS-Earth online calculator (Balco et al., 2008), along with a regional nuclide production rate developed at Lago Argentino, Patagonia (50°S; Kaplan et al., 2011), which is statistically indistinguishable from the other Southern Hemisphere midlatitude production rate, from New Zealand (Putnam et al., 2010).

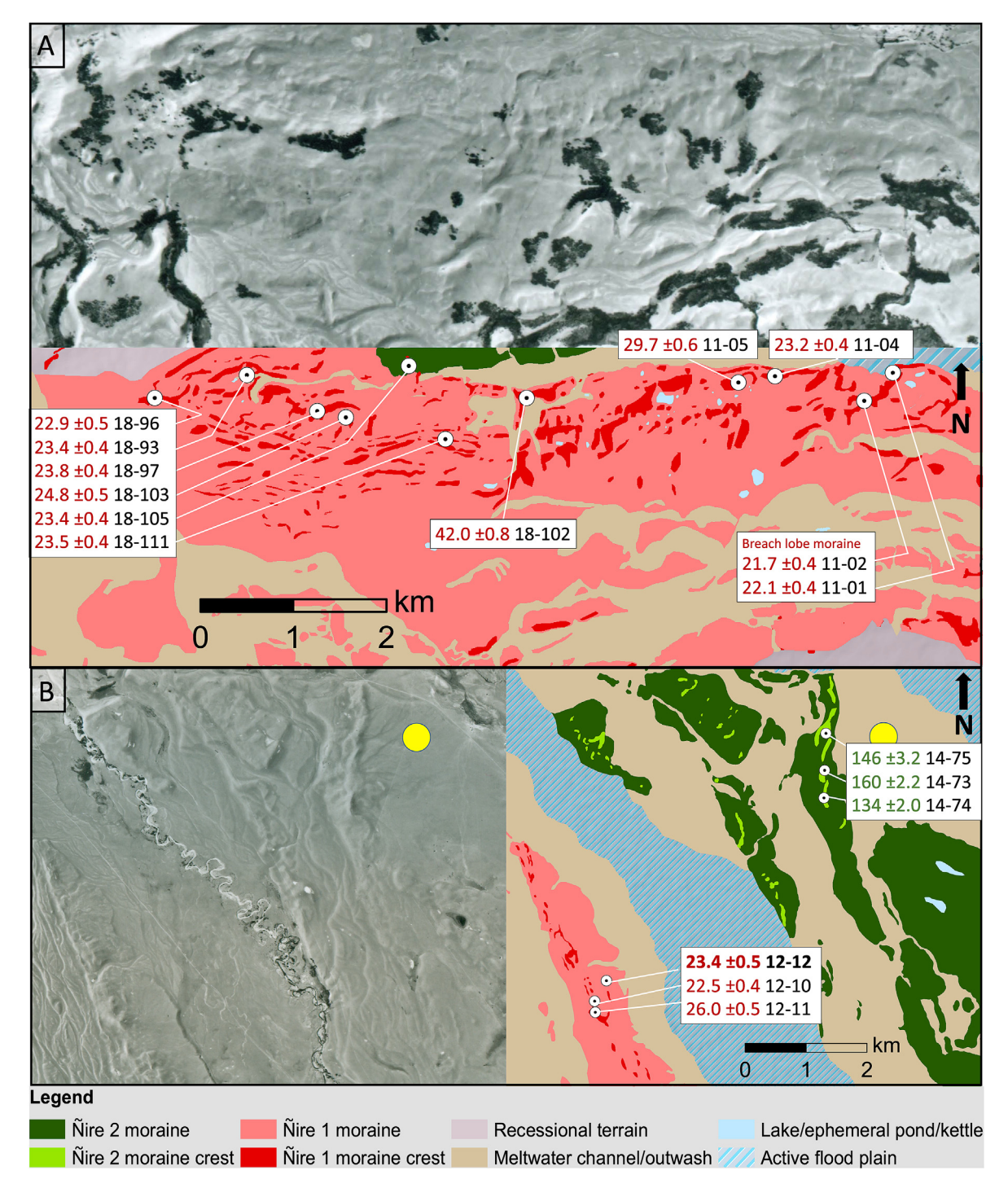


Fig. 3. Comparison between the geomorphic map and the Servicio Aerofotogramétrico de la Fuerza Aérea de Chile photos used for the mapping. A. Ñire 1 moraine sequence showing the left lateral moraines of the main lobe and photo number 010488. Beheaded channels are abundant in the south eastern quadrant. B. Ñire 1 and 2 frontal moraine area (same area as in Fig. 2C) and photo number 010521. Yellow dot marks the location of Fig. 5. (For interpretation of the references to colour in this figure legend, the reader is referred to the Web version of this article.)

We measured topographic shielding (which is negligible for most samples in this study) using a compass and clinometer. We calculated the ages assuming a rock density of 2.65 g/cm³ and using the non-time-dependent scaling (St) from Stone (2000), the time dependent scaling (Lm) of Stone/Lal (Lal, 1991; Stone, 2000), and the LSDn scaling of Lifton et al. (2014) based on modeled fluxes of cosmic-rays. We discuss ages calculated using the Lm scaling scheme in the text, as the ¹⁰Be ages scaled with the Lm scheme

agree most closely with the ¹⁴C data from the Puerto Bandera site at Lago Argentino used in the local production rate calculation (Kaplan et al., 2011), however the choice of scheme does not impact the main conclusions, as even the pre-MIS 6 moraine means calculated using the three schemes overlap within error (Table 2). For comparison, we apply erosion rates of 0.2 mm/kyr (derived in Douglass et al., 2007 for Lago Buenos Aires) and 1 mm/kyr (cf., approximately the maximum rate in Kaplan et al., 2005), however



Fig. 4. Tuff cones forming crag and tails, with till wedges deposited on the downflow sides, in the central Nirehuao basin. The tuff cone in the foreground is marked with an orange dot in Fig. 2A. (For interpretation of the references to colour in this figure legend, the reader is referred to the Web version of this article.)

Table 1 Geographical and analytical data for 10 Be age calculation. Boron-corrected 10 Be/ 9 Be values were measured against the 07KNSTD AMS standard with a reported 10 Be/ 9 Be value of 2.85 × 10¹² (Nishiizumi et al., 2007; 10 Be half-life = 1.36 Myr). 1 $^{\circ}$ analytical or internal AMS uncertainties are shown. Density = 2.65 g/cm³. 10 Be concentrations are corrected for 10 Be in process blanks run with each sample batch. Carrier concentrations in ppm as follows, with the 10 Be/ 9 Be ratios measured in the process blanks in each sample batch: (a) 1032.4, 3.50265 × 10⁻¹⁶, (b) 1034.7, 3.3345 × 10⁻¹⁶, (c) 1031.96, 6.97965 × 10⁻¹⁶, (d) 1045.65, 2.91555 × 10⁻¹⁶, (e) 1036.63, 1.33095 × 10¹⁶.

Sample	CAMS no.	Latitude	Longitude	Elevation	Thickness	Shielding	Boulder ht.	Quartz wt.	⁹ Be Carrier	¹⁰ Be/ ⁹ Be (10 ⁻¹⁴)		¹⁰ Be Concentration		
		(DD)	(DD)	(masl)	(cm)		(cm)	(g)	(g)			$(10^5 \text{ atoms g}^{-1})$		
BN-18-87	BE48466	-45.13616	-71.55052	959	1.6	0.9969	160	4.3195	0.1782 a	$7.555 \pm 0.$.1510	2.141	±	0.0429
BN-18-93	BE48467	-45.17300	-71.57390	1047	1.8	1.0000	175	10.6368	0.1787 ^a		.3682	2.298	±	0.0426
BN-18-96	BE48468	-45.17146	-71.56496	990	1.8	0.9963	190	10.2284	0.1768 a		.3504	2.140	±	0.0417
BN-18-97	BE48469	-45.17390	-71.55815	980	1.8	0.9985	130	10.6626	0.1795 a		.3534	2.213	±	0.0410
BN-18-103	BE48471	-45.17434	-71.55540	967	1.2	0.9927	130	10.6287	0.1808 ^a	19.460 ± 0.0	.3602	2.280	\pm	0.0422
BN-18-105	BE48472	-45.17083	-71.54933	968	1.0	1.0000	112	11.1893	0.1809 a	19.440 ± 0.0	.3601	2.165	±	0.0401
BN-18-111	BE48473	-45.17580	-71.54578	959	1.4	1.0000	164	10.4362	0.1788 a	18.227 ± 0.0	.3378	2.151	±	0.0399
BN-14-58	BE40574	-45.18441	-71.49330	818	2.6	0.9999	180	3.5591	0.1810 ^d	5.490 ± 0.0	.1141	1.941	±	0.0424
BN-14-59	BE40575	-45.18233	-71.48795	824	2.7	0.9998	70	6.0835	0.1813 ^d	8.990 ± 0.0	.1764	1.866	±	0.0374
BN-14-61	BE40576	-45.18139	-71.48859	823	1.2	0.9996	65	6.0637	0.1814 ^d	9.094 ± 0.0	.1820	1.895	±	0.0387
BN-14-63	BE44392	-45.18713	-71.46608	878	0.7	1.0000	70	15.1959	0.1813 ^b	$24.755 \pm 0.$.4107	2.040	±	0.0339
BN-14-64	BE44393	-45.18710	-71.46573	875	1.2	1.0000	150	15.0385	0.1811 ^b	$25.237 \pm 0.$.4708	2.099	±	0.0392
BN-14-70	BE44394	-45.17658	-71.48061	890	1.2	1.0000	120	15.0106	0.1806 ^b	25.369 ± 0.0	.4718	2.108	±	0.0392
BN-12-12	BE44391	-45.20801	-71.43912	869	0.8	1.0000	148	15.1022	0.1814 ^b	$24.174 \pm 0.$.5357	2.005	±	0.0445
BN-11-04	BE38230	-45.17153	-71.51388	935	1.2	1.0000	105	9.0687	0.1818 ^e	15.049 ± 0.0	.2565	2.088	±	0.0358
BN-12-10	BE44389	-45.21016	-71.44085	890	1.1	1.0000	124	15.0703	0.1807 ^b	23.609 ± 0.0	.4410	1.955	±	0.0365
BN-12-11	BE44390	-45.21130	-71.44076	892	1.4	1.0000	166	8.8198	0.1821 b	$15.908 \pm 0.$.2967	2.267	±	0.0424
BN-11-01	BE38228	-45.17131	-71.50249	915	0.7	1.0000	152	8.8289	0.1820 e	$13.739 \pm 0.$.2712	1.960	±	0.0389
BN-11-02	BE38229	-45.17320	-71.50525	925	1.0	1.0000	125	9.0620	0.1822 ^e	$13.893 \pm 0.$.2744	1.933	±	0.0384
BN-12-06	BE44387	-45.18219	-71.46511	900	0.9	1.0000	94	15.1377	0.1786 ^b	23.789 ± 0.0	.4356	1.938	±	0.0355
BN-12-07	BE44388	-45.18204	-71.46561	907	1.4	1.0000	100	15.1427	0.1804 ^b	19.231 ± 0.	.3879	1.582	±	0.0319
BN-11-05	BE38231	-45.17197	-71.51744	947	0.6	1.0000	70	9.4516	0.1826 ^e		.4038	2.738	±	0.0541
BN-18-102	BE48470	-45.17300	-71.53791	953	2.1	1.0000	128	11.0295	0.1803 a	$34.227 \pm 0.$.6318	3.857	±	0.0712
BN-14-45	BE40571	-45.13702	-71.50857	1016	1.6	1.0000	170	3.8816	0.1813 ^d	44.873 ± 0.0	.6546	14.638	±	0.2139
BN-14-49	BE43864	-45.13854	-71.51606	1048	0.7	1.0000	100	7.0584	0.1818 ^c	83.275 ± 1.	.1267	14.781	±	0.2000
BN-14-51	BE43865	-45.14336	-71.53964	1030	1.8	1.0000	160	7.1886	0.1811 ^c	85.922 ± 1.	.1610	14.918	±	0.2016
BN-14-55	BE40572	-45.16156	-71.52239	957	1.3	1.0000	190	6.1019	0.1813 ^d	67.637 ± 1.	.0788	14.039	±	0.2240
BN-14-73	BE43867	-45.18611	-71.40688	928	0.9	1.0000	110	7.0746	0.1813 ^c	80.927 ± 1.	.0782	14.292	±	0.1905
BN-14-75	BE43869	-45.18227	-71.40669	935	1.0	1.0000	100	7.0324	0.1812 ^c	74.078 ± 1.	.5589	13.153	±	0.2768
BN-14-44	BE43863	-45.13795	-71.50657	1014	1.8	1.0000	160	7.1105	0.1812 c			13.183	±	0.1784
BN-14-57	BE40573	-45.16096	-71.51919	956	1.5	1.0000	130	1.8205	0.1813 d			12.504	±	0.2452
BN-14-74	BE43868	-45.18900	-71.40698	932	1.3	1.0000	100	7.0194	0.1817°			12.024	±	0.1718
BN-14-41	BE40570	-45.12449	-71.51689	1079	1.1	0.9999	100	6.0449	0.1802 ^d			17.730	±	0.3385
BN-14-31	BE43861	-45.13109	-71.50425	1070	1.2	1.0000	50	7.1575	0.1812 ^c			19.872	±	0.2687
BN-14-36	BE44396	-45.12628	-71.52052	1067	2.6	0.9999	70	7.1614	0.1803 b			19.604	±	0.2883
BN-14-28	BE43860	-45.12982	-71.50895	1085	1.1	0.9991	100	7.0370	0.1830 ^c			16.114	±	0.2178
BN-14-38	BE43862	-45.12074		1124	2.1	0.9999	320	7.1926	0.1816°	_		27.144	_	0.3669

we argue the ages calculated without an erosion rate are the most accurate (see discussion section 6). We calculated mean ages for moraines and present them with the standard deviation and the propagated error on the production rate of 3% (Kaplan et al., 2011). For individual ages, the noted uncertainties are 1 σ analytical uncertainties. Ages excluded from the moraine means are either more than two standard deviations from the mean, or are out of

morphostratigraphic order and are more than one standard deviation from the mean. We recalculated all ¹⁰Be ages from prior publications using the same systematics to allow us to make meaningful comparisons.

Lastly, we also retrieved multiple overlapping piston cores from Lago Mano Negra (Fig. 1B; 45°23′19.12″S, 71°55′13.18″W, 840 masl) using a square-rod Livingstone corer (Wright et al., 1984). The lake

sits in a small closed-basin depression $\sim\!42~\text{km}$ upstream from the Nirehuao terminal moraines.

5. Results

The northern margin of the Ñirehuao valley contains a long sequence of moraines and glaciofluvial deposits, marking the terminal extents of two sub-lobes, the smaller, northern sub-lobe, and the larger, main sub-lobe to the south (outlined by the red dashed line in Fig. 1B), which together form the Ñirehuao lobe. The sub-lobes are separated by an east-west trending bedrock ridge that has a saddle just west of the study area (labeled "Saddle" in white

text on Fig. 1B) with an elevation of ~760 masl (currently incised by the Río Ñirehuao). This is well below the elevation of even the lowest outboard moraines, suggesting that the two sub-lobes converged at thicknesses above ~760 masl, just south of the study area. Just outside (hereafter, outboard) of the saddle, the sub-lobes bifurcate into two margins, the northern sub-lobe and the main sub-lobe, forming a "V" shaped sequence in the moraine complexes between the two sub-lobes, which we refer to here as the interlobe area. Ice likely also flowed into the Ñirehuao valley from Valle Richiardi (Fig. 1B) and converged with the Ñirehuao glacier lobe just to the southwest of the mapped extent.

Table 2

10 Be ages (ka) calculated using the non-time-dependent scaling (St) from Stone (2000)/Lal, (1991), the time dependent scaling (Lm) of Stone/Lal, and the LSDn scaling of Lifton et al. (2014). Ages calculated using Lm are discussed. Mean moraine ages (shown in bold and underlined) include samples in bold and exclude samples in italics, and are shown with the standard deviation and propagated 3% error of the production rate (Kaplan et al., 2011). Samples were run at CAMS with the 07KNSTD standard. No correction for snow cover or erosion was made to these data. The effect of applying an erosion rate is shown in Table 3.

Moraine group	Sample	Age (St)	Age (LSDn)	Age (Lm)		
		(ka)	(ka)	(ka)		
	BN-18-87	24.2 ± 0.5	23.4 ± 0.5	23.5 ± 0.5		
	BN-18-93	24.2 ± 0.5	23.3 ± 0.4	23.4 ± 0.4		
Northern sub-lobe Ñire 1	BN-18-96	23.7 ± 0.5	22.9 ± 0.4	22.9 ± 0.5		
	<u>Mean</u>	24.0 ± 0.8	23.2 ± 0.8	23.3 ± 0.8		
	BN-18-97	$\textbf{24.6} \pm \textbf{0.5}$	$\textbf{23.7} \pm \textbf{0.4}$	$\textbf{23.8} \pm \textbf{0.4}$		
	BN-18-103	25.6 ± 0.5	24.7 ± 0.5	24.8 ± 0.5		
	BN-18-105	24.1 ± 0.5	23.3 ± 0.4	23.4 ± 0.4		
	BN-18-111	24.2 ± 0.5	23.4 ± 0.4	23.5 ± 0.4		
	BN-14-58	24.8 ± 0.5	24.0 ± 0.5	24.0 ± 0.5		
	BN-14-59	23.7 ± 0.5	23.1 ± 0.5	23.0 ± 0.5		
	BN-14-61	23.8 ± 0.5	23.2 ± 0.5	23.1 ± 0.5		
	BN-14-63	24.4 ± 0.4	23.6 ± 0.4	23.6 ± 0.4		
	BN-14-64	25.3 ± 0.5	24.4 ± 0.5	24.4 ± 0.5		
Main sub-lobe Ñire 1 (left lateral moraine)	BN-14-70	25.1 ± 0.5	24.2 ± 0.5	24.3 ± 0.5		
	BN-11-04	23.9 ± 0.4	23.2 ± 0.3 23.2 ± 0.4	23.2 ± 0.4		
	BN-11-01	22.7 ± 0.5	23.2 ± 0.4 22.1 ± 0.4	23.2 ± 0.4 22.1 ± 0.4		
	BN-11-02	22.3 ± 0.4	21.7 ± 0.4	21.7 ± 0.4		
	BN-12-06	22.8 ± 0.4 22.8 ± 0.4	21.7 ± 0.4 22.1 ± 0.4	22.1 ± 0.4		
	BN-12-07	18.5 ± 0.4	18.3 ± 0.4	18.2 ± 0.4		
	BN-11-05	31.0 ± 0.6	29.5 ± 0.6	29.7 ± 0.6		
	BN-18-102	44.1 ± 0.8	23.3 ± 0.0 41.6 ± 0.8	42.0 ± 0.8		
	Mean		23.7 ± 0.9	23.7 ± 0.9		
	Wean	<u>24.5 ± 1.0</u>	<u>23.7 ± 0.9</u>	<u>23.7 ± 0.9</u>		
	BN-12-12	$\textbf{24.1} \pm \textbf{0.5}$	$\textbf{23.4} \pm \textbf{0.5}$	$\textbf{23.4} \pm \textbf{0.5}$		
Main sub-lobe Ñire 1 (frontal moraine)	BN-12-10	23.2 ± 0.4	22.5 ± 0.4	22.5 ± 0.4		
	BN-12-11	26.9 ± 0.5	25.9 ± 0.5	26.0 ± 0.5		
Main sub-lobe Ñire 1 (all)	<u>Mean</u>	<u>24.5 ± 1.0</u>	$\underline{23.7} \pm \underline{0.9}$	$\underline{23.7} \pm \underline{0.9}$		
Both Ñire 1 sub-lobes	<u>Mean</u>	24.4 ± 0.9	$\underline{23.6} \pm \underline{0.9}$	23.6 ± 0.9		
	BN-14-45	$\textbf{163} \pm \textbf{2.5}$	150 ± 2.3	$\textbf{153} \pm \textbf{2.3}$		
	BN-14-49	159 ± 2.2	147 ± 2.1	150 ± 2.1		
	BN-14-51	165 ± 2.3	152 ± 2.1	155 ± 2.2		
Ñire 2	BN-14-55	164 ± 2.7	151 ± 2.5	154 ± 2.6		
Moraine ridges	BN-14-73	170 ± 2.4	158 ± 2.2	160 ± 2.2		
	BN-14-75	155 ± 3.4	144 ± 3.1	146 ± 3.2		
	<u>Mean</u>	<u>163 ± 5.4</u>	150 ± 5.1	<u>153 ± 5.1</u>		
	BN-14-44	147 ± 2.1	$\textbf{135} \pm \textbf{1.9}$	$\textbf{138} \pm \textbf{1.9}$		
Ñire 2	BN-14-57	146 ± 3.0	134 ± 2.7	137 ± 2.8		
Channel margins	BN-14-74	142 ± 2.1	132 ± 1.9	134 ± 2.0		
manuer margins	Mean	142 ± 2.7 146 ± 4.5	132 ± 1.5 134 ± 4.1	137 ± 4.2		
	····cuii	110 <u>+</u> 1.0	137 <u>T</u> 7.1			
	BN-14-41	$\textbf{188} \pm \textbf{3.8}$	$\textbf{173} \pm \textbf{3.5}$	$\textbf{177} \pm \textbf{3.5}$		
	BN-14-31	$\textbf{214} \pm \textbf{3.1}$	$\textbf{195} \pm \textbf{2.8}$	$\textbf{200} \pm \textbf{2.8}$		
Ñire 3	BN-14-36	$\textbf{214} \pm \textbf{3.3}$	$\textbf{195} \pm \textbf{3.0}$	$\textbf{200} \pm \textbf{3.1}$		
	BN-14-28	170 ± 2.4	156 ± 2.2	159 ± 2.2		
	<u>Mean</u>	<u>206 ± 16</u>	<u>188 ± 14</u>	<u>192 ± 15</u>		
Outermost Ñire 3	BN-14-38	288 ± 4.2	260 ± 3.8	267 ± 3.9		

5.1. Geomorphic mapping

We present a highly detailed geomorphic map of the northern sector of the Ñirehuao valley and the deposits left by the former northern and main sub-lobes, which together form the Ñirehuao lobe. The map is centered at ~45.2°S, 71.5°W and covers an area of ~30 \times 10 km.

5.1.1. Moraine complexes

Three distinct moraine complexes comprise the most prominent landforms in the study area and are classified as Nire 1 (innermost; mapped in pink in Fig. 2), Nire 2 (intermediate; green), and Nire 3 (outermost; blue). Moraine complexes are groups of moraines. Moraines are areas of positive relief with an arcuate (valley-wide scale) to linear (smaller scale) shape (Fig. 2A). They are separated from each other along their long axes by meltwater channels and outwash plains, and frequently on their short axes by modern channels.

The Nire 1 moraine has two sub-lobes connected by a "V" shaped interlobe moraine area. The Ñire 1 moraine is the most well preserved and has a width reaching ~2 km across (i.e., parallel to the paleo ice flow direction). It has a sequence of smaller scale moraine areas of positive relief, with heights of ~1-10 m and widths of <20 m. The ice proximal slope of the left lateral Ñire 1 moraine of the main sub-lobe has a southern aspect, with a maximum slope of ~70 m/km. The slope becomes gentler towards the frontal position, with values around ~20 m/km. Some areas of the Nire 1 moraine complex are imprinted with kettle holes, and in a few small areas with kettle and kame topography. We do not map these areas as kettle and kame topography, as these landforms are first and foremost part of the moraine complex demarcating the margins of the ice lobe, which is the primary intended use of this map; instead, we map the overprinted kettle holes on the moraine complex (e.g. Soteres et al., 2020).

The Nire 2 moraine complex appears to have followed the same general "V" pattern in the interlobe area but extending farther east. The Nire 2 complex consists of elevated moraine, the most prominent of which stands up to ~110 m above the surrounding outwash, with widths up to ~2 km. The Nire 2 moraine crests are heavily dissected by outwash (more so than on the Nire 1 moraine). The Nire 1 and Nire 2 complexes are most well preserved at the higher elevations (~1040 - 960 m) where the two sub-lobes met, towards the center of the study area, and are progressively more dissected by glaciofluvial landforms towards the southeast and frontal moraines.

A similar concentric curve shape is also apparent in the next outermost complex (Nire 3), but only left lateral moraines associated with the Nire 3 complex are preserved within the study area. The Nire 3 complex consists of a gently curved array of low-relief, irregular topography cut by channels. These moraines are broad and flat with notably less surface relief than the other complexes, where moraine crests largely stand <5 m above the moraine surface. Finer scale relief and landforms such as kettle holes and ponds are absent. This complex is also located at higher elevations (above ~1050 m) relative to the Nire 2 moraine complex.

Moraine crests mark the tallest linear ridges of the moraines and are discernible in stereopair imagery. The moraine crests are discontinuous, where Ñire 1 crests have lengths of ~10–500 m, in some areas potentially reflecting variable loads of glacial debris along the margin of the glacier (Benn and Evans, 2014), and in others, the post-depositional cross-cutting by meltwater. The Ñire 1 landform complex contains a series of at least 6 definable and geomorphologically distinct moraine crests. Mapping moraine crests at such a fine scale allows us to identify small scale features like breach lobe moraines (described in section 6.1.3 and labeled in

Fig. 3A with samples 11–02 and 11–01). The older moraines tend to have longer and wider moraine crests as the finer structure is not as well preserved. The moraine crests on the Ñire 2 and 3 moraines extend up to 1 km in length and predominantly have widths in the tens of meters but occasionally are as wide as 200 m.

5.1.2. Recessional terrain

There is a large overdeepened basin (Fig. 1B) inside the major terminal margins where it appears the main sub-lobe occupied while depositing the Nire 1 moraine. This area is occupied by subglacial landforms, including flutes, grooves, and ribbed moraine. These features are not mapped individually as the focus of this work is the glacial maximum ice margins. We refer the reader to Cooper et al. (2021) who mapped features in this recessional terrain area.

5.1.3. Shorelines

Shorelines are long, flat-topped ridges that often appear in sets and typically extend over long distances. At least four major shorelines in the area are preserved at ~750 masl, ~740 masl, ~730 masl, ~720 masl. A longer sequence of shorelines (at least 20) can be seen on many hills with valley-facing aspects, with elevations from 750 to 560 masl. The most prominent paleolake shoreline occurs at ~740 masl and is clearly defined in the landscape (Fig. 2A).

5.1.4. Outwash plains

Gently sloping (\sim 0.1%) wide areas (up to \sim 5 km) of glaciofluvial sand and gravel are mapped as outwash plains. Networks of braided meltwater channels are well-preserved on the farthest inboard outwash plains and are less apparent on the farther outboard plains. The outwash plains associated with the Nire 2 moraines are covered by a well-developed soil layer in post-glacial sediment, \sim 50 cm thick (Fig. 5). Outwash plains are most abundant towards the frontal margin (easternmost sector of the study area), heavily dissecting the Nire 2 moraine complex.

5.1.5. Meltwater channels

Meltwater channels are intimately associated with outwash plains, they frequently are crosscut by, feed into, and overprint outwash plains. Meltwater channels are straight to sinuous and can be braided. They have dull, rounded scarps as compared to the modern channels, and sometimes host modern drainage and wetlands. They often originate from former ice-margin positions and do not follow modern topography, often cross-cutting moraines. Beheaded meltwater channels (i.e. channels whose endpoints have been eroded; Fig. 3) are abundant in the area, and can record the final thinning and retreat of the glacier down the ice contact slope.

5.1.6. Lakes/ponds/kettles

Standing water is grouped together in this category. Ephemeral ponds and kettles are abundant, as some are filled in with water in the more recent satellite images but are bog/peatland in aerial photos. Closed basins in formerly glaciated areas can be produced by a number of processes or events, and we refer the reader to the Cooper et al. (2021) where lakes and kettle holes are distinguished.

5.1.7. Ice-molded bedrock

Ice-molded tuff cones are abundant in the valley and frequently have tails of till on the downflow side (Fig. 4). The tallest cones have elevations of ~760 masl similar to the highest paleolake shoreline elevations. The underlying bedrock can be seen outcropping along the inside of the $\tilde{\text{Nire}}$ 1 terminal margin.



Fig. 5. Depth profile through the N̄ire 2 outwash plain. The upper 50 cm includes a soil cover that we infer developed mainly in post-glacial sediment that grades downward into relatively unweathered outwash sediments. Location of site marked with a yellow dot in Fig. 2A. (For interpretation of the references to colour in this figure legend, the reader is referred to the Web version of this article.)

5.2. Chronology

We present thirty-seven new ¹⁰Be dates (Table 1), and their geographical and analytical data (Table 2). Moraine statistics are represented in normal kernel density estimates shown in Fig. 7.

Twenty-one new 10 Be ages from the Ñire 1 moraines fall within MIS 2. The northern sub-lobe has a mean age of 23.3 ± 0.8 ka (n = 3) and the left lateral moraines of the main sub-lobe date to 23.7 ± 0.9 ka (n = 11, 6 excluded). All together these ages range from 24.8 ka to 22.5 ka and produce a mean age of 23.6 ± 0.9 ka (n = 15; 6 ages excluded; 23.3 ± 1.5 ka with all ages included). The frontal moraines of the main sub-lobe (Fig. 2C) have a larger age range, but cluster around the mean of the lateral moraines nonetheless. On an outermost crest of the Ñire 1 moraine, we date one boulder (BN-18-102) on a moraine geomorphically separate from the MIS 2-dated moraine crests to 42.0 ± 0.8 ka. Just to the east, the next boulder we sampled produced an age of 29.7 ± 0.6 ka.

Outboard of the Ñire 1 moraine, there is another set of moraines, Ñire 2, that are clearly distinguishable from the inboard moraine in aerial imagery by the more subdued relief. We date the left lateral and interlobe moraines to 153 ± 5.1 ka (n=4). Two dates in this area obtained from boulders on the margins of meltwater channels yield a mean age of 137 ± 4.2 ka. To the south, we dated three boulders from the frontal moraines which, similar to the ages from the inboard frontal Ñire 1 moraine, have a larger range in ages $(160 \pm 2.2$ ka $- 134 \pm 2.0$ ka) but cluster around the moraine means of the northern lobe (Fig. 2) and produce a mean of 153 ± 9.9 ka

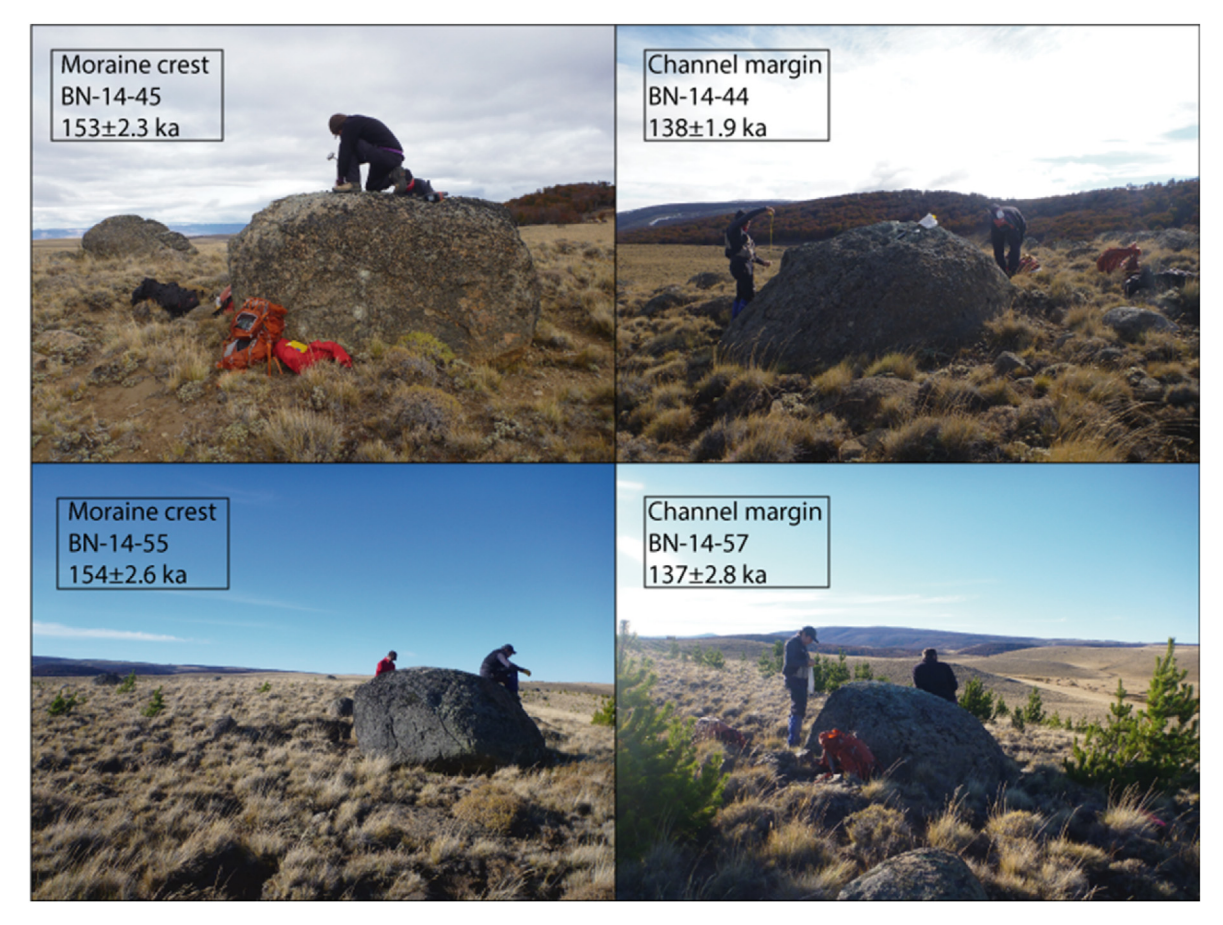


Fig. 6. Examples of four boulders selected for sampling. The left two photos show examples of boulders on moraine crests, and the right two photos show examples of nearby boulders (within 300 m) on the edges of the moraines bordering meltwater channels. Note the higher gradient of the moraine surface on the right two photos as compared to the flatter moraine crest of the left two photos. Also note the abundance of cobbles and boulders on the channel margin surface, suggesting these two surfaces may have had their finer surface sediments removed

(n = 2; 1 age excluded).

Outboard of the Nire 2 moraine, the higher elevation, more diffuse Nire 3 moraines curve around the small, northern lobe of the Nire 2 moraine. We dated four boulders on these moraines with an average age of 192 ± 15 ka (n = 3; 1 outlier excluded). Just outboard of this, the outermost, highest elevation sample we collected produced an age of 267 ± 3.9 ka. Beyond the mapped and dated frontal moraines are at least 2 more unstudied moraine limits (Fig. 1B).

For comparison, we also calculate the ages using boulder erosion rates of 0.2 mm/kyr (Douglass et al., 2007) and 1.0 mm/kyr (Table 3) as discussed in the methods section. This increases the Ñire 1 moraine age to 23.7 ± 0.9 and 24.1 ± 0.9 ka, the Ñire 2 channel age to 141 ± 4.3 and 156 ± 4.8 ka, the Ñire 2 crest age to 157 ± 5.3 and 177 ± 6.1 ka, the inner Ñire 3 to 199 ± 16 and 233 ± 22 ka and lastly, the outermost Ñire 3 age to 280 ± 9.4 and 358 ± 13 ka.

5.3. Lake sediment coring

Lago Mano Negra sits in a small closed-basin depression on the foothills of Cerro Mano Negra, approximately 300 m above the Río Emperador Guillermo valley floor, ~42 km upstream from the Ñire 1 moraines, ~12 km southwest and ~300 m below Lago La Trapananda (Weller et al., 2019). The sedimentary record from Lago Mano Negra includes a ~2.5 m-thick basal glaciolacustrine unit, overlain by ~6.5 m of organic lake mud with multiple tephra layers. A basal radiocarbon age of 15,300 \pm 90 years (CAMS-186294) affords a minimum limiting age for the onset of organic lake deposition at ~18.5 cal ka BP (2σ range =18.3-18.8 cal ka BP). This age is supported by additional dates further up the stratigraphy (Villa-Martínez & Moreno, in prep.).

6. Discussion

The Ñirehuao valley records at least three advances of the Patagonian Ice Sheet, one during MIS 2, two during MIS 6 and one potentially during MIS 8 (at least one age), allowing us to understand the regional terrestrial glacier response to global climate changes during glacial periods. Here we discuss our moraine chronology from oldest to youngest, the climate implications of our record, and highlight areas of opportunity for future study.

Prior broad-scale mapping efforts (Caldenius, 1932; García et al., 2019; Cooper et al., 2021) mapped the Ñirehuao moraine sequence as all left lateral moraines, which would lead to incorrect interpretations on their morpho-stratigraphic order. We find that during MIS 2 and MIS 6 there were two sub-lobes that terminated in this area, leading to a more nuanced moraine morphostratigraphic order. We suggest that the northern sub-lobe merged with the main sub-lobe at the saddle (Fig. 1B) and then diverged at the terminus around the bedrock ridge (Fig. 2A). It is

Table 3Moraine average ages (ka) calculated with no boulder erosion, 0.2 mm/kyr erosion (Douglass et al., 2007) and 1.0 mm/kyr (cf. the maximum erosion rate from Kaplan et al. (2005)). All averages are shown with their standard deviation and the propagated production rate error.

	Erosion rate (mm/kyr):								
	0			0.2			1		
Ñire 1 (n = 15)	23.6	±	0.9	23.7	±	0.9	24.1	±	0.9
\tilde{N} ire 2 channels (n = 2)	137	±	4.2	141	±	4.3	156	±	4.8
\tilde{N} ire 2 ridges (n = 4)	153	±	5.1	157	±	5.3	177	±	6.1
\tilde{N} ire 3 (n = 3)	192	±	15	199	±	16	233	±	22
Outermost \tilde{N} ire 3 (n = 1)	267	±	8.9	280	±	9.4	358	±	13

unclear whether the two sub-lobes were fully merged during the prior advance because only left lateral moraines are preserved; the right lateral margin of the smaller northern sub-lobe (i.e., the interlobe moraine) and left lateral moraines of the main sub-lobe may have been overrun by the advance associated with the Nire 2 moraine.

We discuss the ages without a correction for boulder erosion rather than apply a single poorly constrained rate to all of the data for the following reasons: first, applying a poorly constrained erosion rate has been demonstrated to reduce the accuracy of some datasets (Gillespie and Bierman, 1995). Second, erosion rates are likely quite variable between boulders and between sites (i.e. applying an erosion rate derived from a different study site may not be appropriate). Third, we only collected samples from what appear to be original boulder surfaces (i.e. surfaces that appear to have remained intact and not eroded since they were deposited). Fourth, we used an empirically derived production rate from Lago Argentino, also on the east side of the Andes, that most likely experienced similar average boulder erosion rates. Hence, the effects of erosion are already incorporated in the age calculations, at least during the MIS 2 portion of the record. Furthermore, moraine erosion/degradation is also implicitly included in some erosion rate values in addition to boulder erosion (e.g. the Kaplan et al. (2005) erosion rate is based on 40Ar/39Ar independent age constraints of the moraines and therefore the erosion rate includes any process that makes the boulder exposure ages younger than the moraines). We note that transects dug into an outwash plain in the study area demonstrated that the matrix appears to have undergone net aggradation over this time period rather than net deflation (Fig. 5). which might have limited the moraine degradation in Nirehuao. We also note that the higher erosion rate in Kaplan et al. (2005) is based on cobbles and boulders that all have heights of 55 cm or less and the Nirehuao ages come from taller boulders (Fig. 8). For these reasons, we do not use an erosion correction as the ages may be more accurate without an erosion rate applied. Nevertheless, we do show the data with two erosion rates applied to allow visualization of their impacts (Table 3).

6.1. Moraine chronology

6.1.1. Pre-MIS 2 chronology

The farthest outboard sample (BN-14-38) produced an age of 267 ± 3.9 ka, overlapping with MIS 8 (300-243 ka). This date comes from the highest elevation sample we collected (it is 40 m higher than the next highest sample, BN-14-28), and also from the tallest boulder we sampled (320 cm). It is from a moraine crest that is geomorphologically distinct from the inboard moraine crests that produce younger ages.

The four ages from the moraines between the Nire 2 moraine and the boulder dated to MIS 8 are less straightforward. The boulder age of 159 \pm 2.2 ka is considered an outlier, and likely has incomplete exposure as it is younger than inboard samples. Two boulders from this area produce identical ages of 200 \pm 3 ka and are in morphostratigraphic order with the rest of the ages, suggesting they could reflect the age of a glacier advance. However, they could also represent minimum ages for an older advance in light of (1) the scatter of the four ages, (2) the findings of Hein et al. (2017) of some moraine ages in other sites dramatically underestimating moraine formation age, and (3) the fact that we do not apply an erosion rate correction. Further study of this time period and a possible advance at ~200 ka is warranted. While these ages do not offer sufficient precision to resolve the exact timing of the glacier advances associated with the Nire 3 moraine formation, they at least provide minimum ages for the glacial events predating the main MIS 6 advance (see below).

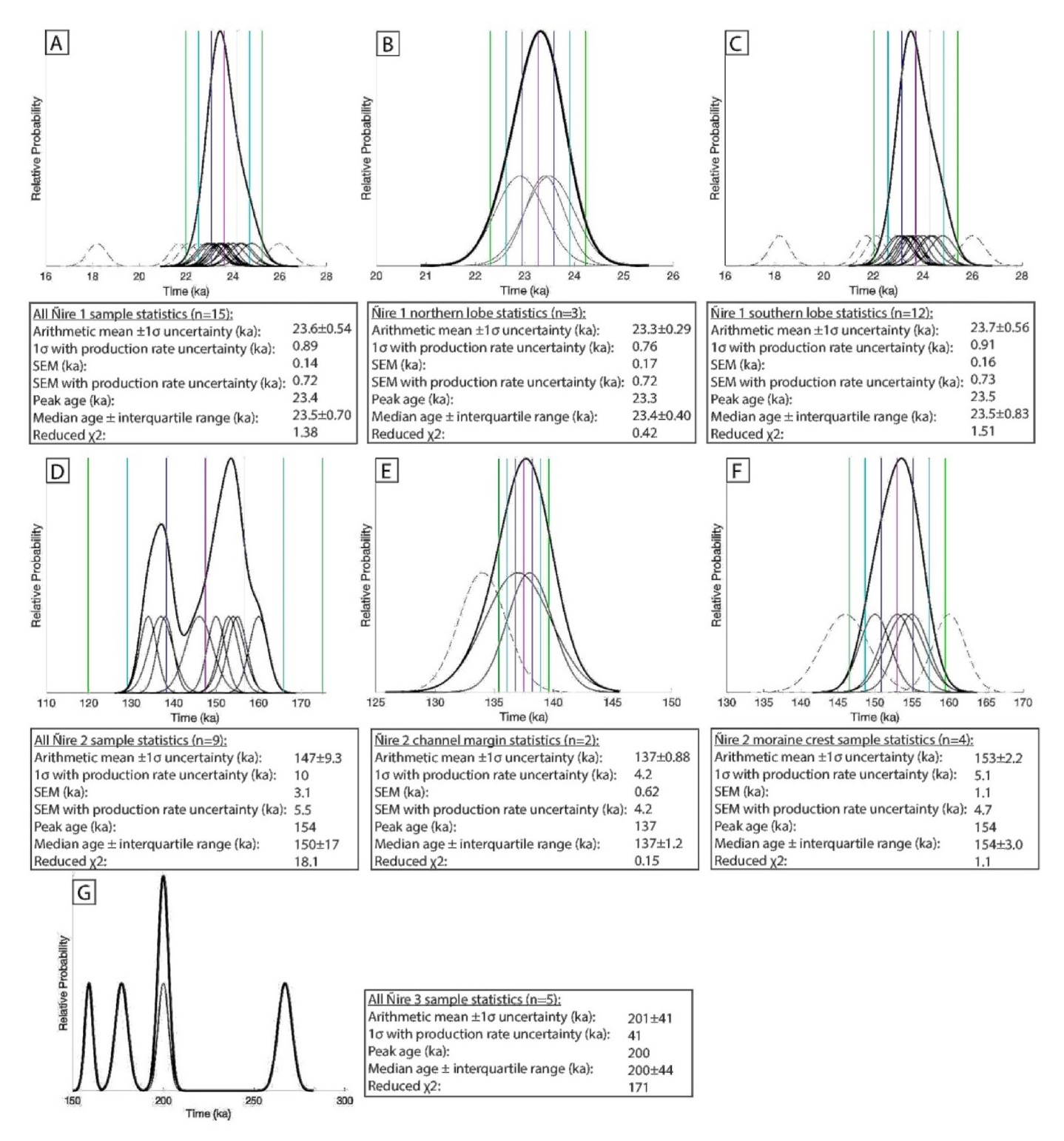


Fig. 7. 10 Be ages and descriptive statistics for the moraine sequence at Nirehuao. Thin black lines are normal kernel density estimates of individual samples with their 1 σ internal error. Thick lines are the sums of the individual curves. Dashed curves are excluded from the summed curve. Pink vertical lines are the mean ages. The blue, cyan and green vertical lines are the 1, 2, and 3 σ bounds respectively. Standard error of the mean (SEM) is also included in the table for reference. (For interpretation of the references to colour in this figure legend, the reader is referred to the Web version of this article.)

6.1.2. MIS 6 chronology

Plotted all together (the northern and main sub-lobes with no outliers excluded), the ages from the Ñire 2 moraines (Fig. 2) are bimodal, with 3 ages clustering around ~137 ka, and 6 ages clustering around 153 ka (Fig. 7D). Two ages from the ~137 ka group

come from boulders located on marginal areas of channels that are eroded into the moraine from the northern sub-lobe (Fig. 6), consequently, we plot these ages (Fig. 7E) separate from the moraine crest samples (Fig. 7F). The third date of the channel margin group (BN-14-74; 134 ± 2.0 ka) is from the top of a frontal

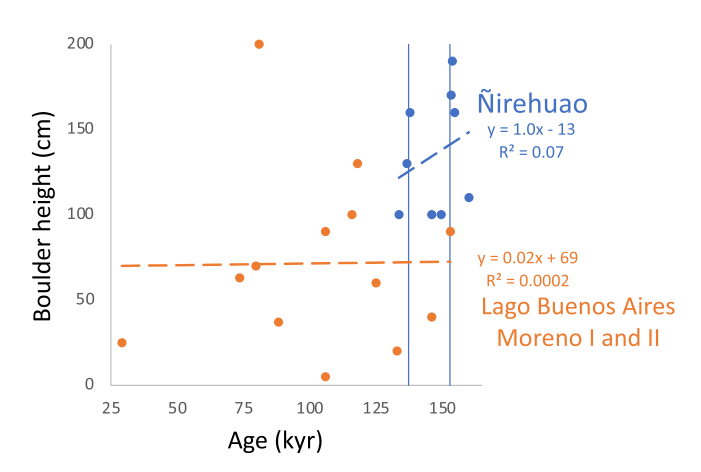


Fig. 8. Comparison between N̄irehuao and Lago Buenos Aires boulder heights and exposure ages. Lago Buenos Aires Moreno I and II data in orange (Kaplan et al., 2005; n=13) and N̄irehuao MIS 6 data in blue (this study; n=9). Blue vertical lines mark the N̄irehuao mean ages of $153\pm5.1\,$ ka and $137\pm4.2\,$ ka. (For interpretation of the references to colour in this figure legend, the reader is referred to the Web version of this article.)

moraine and may be an outlier for the ~153 ka group. Regardless, it is slightly younger than the northern sub-lobe channel margin samples and is not included in the statistics. Altogether, with outliers excluded, these data show that both sub-lobes reached their maximum extents by at least 153 \pm 5.1 ka and were subsequently less extensive. This was followed by a stillstand or smaller readvance that drained via the meltwater channels in this area at 137 \pm 4.2 ka.

While the study site spans a large area with two sub-lobes, where the northern sub-lobe is much narrower and higher elevation (Fig. 1B), the chronology shows that the whole margin formed coevally within dating precision during each glaciation. Furthermore, in the case of both the Nire 1 and Nire 2 deposits, the ages on the frontal moraines of the main sub-lobe (Fig. 2C) correspond with the ages on the northern sub-lobe (Fig. 2B) but with a greater age range and more outliers, potentially reflecting the heavier dissection by meltwater coming off the front of the glacier, as evidenced by the geomorphic mapping. This result suggests that, even in compound piedmont glacier systems with multiple inputs, the generally better-preserved lateral moraines may offer more precision for exposure dating.

It seems unlikely that these MIS 6 dates greatly underestimate the age of the moraines, in part, given their internal consistency. With regard to the Kaplan et al. (2005) study at Lago Buenos Aires that focused on pre-LGM moraine boulders that were later inferred to be ~100 kyr younger than the outwash surfaces associated with the moraine (Hein et al., 2017), we note that when compared with the Nirehuao data, the Lago Buenos Aires data come from shorter samples, are younger and are far more scattered (Fig. 8) and for these reasons perhaps the boulders were exhumed from the moraine surface. We note that there is no statistical correlation between exposure age and boulder height at either site (Nirehuao: $r^2 = 0.07$, p-value = 0.49; Lago Buenos Aires: $r^2 = 0.0002$). Further study with a larger dataset is needed to investigate fully the relationship between boulder height and exposure age for pre-last glacial cycle moraine boulders. We also note that at the Lago Buenos Aires and Pueyrredón sites, in outcrops, outwash surfaces are often capped with a stone-pavement like cover consisting of a high density of cobbles and small boulders often ventifacted (Hein et al., 2009, 2017) and covered in places only by a thin layer of non-glacial material (10–15 cm). The outwash plain bordering the frontal Nire 2 moraine at Ñirehuao on the other hand is covered in vegetation and only a few cobbles per square meter on the surface. The upper 50 cm includes sediment that we assume to be non-glacial in which soil is well developed (Fig. 5). This may be related to the proximity of active volcanoes; Ñirehuao is located in the Southern Volcanic Zone, so it is directly downwind from active volcanoes, while Lago Buenos Aires and Pueyrredón are on the southern border of this chain of volcanoes, in the Patagonian Volcanic Gap (Fig. 1A). The supply of ash may have allowed for net aggradation of the moraine surfaces in the study site, such as on the outwash plain (Fig. 5), maintaining the stability of the moraine boulders, which were not erosionally exhumed.

When the glacier sat at the Ñire 1 margin, its meltwater flowed laterally around the elevated interlobe Ñire 2 moraine. On the outer edge of the Ñire 1 moraine margin is a geomorphically separate moraine crest with a boulder we dated to 42.0 ± 0.8 ka (BN-18-102). This moraine may be the remnant of a pre-MIS 2 advance, where, in this higher elevation bedrock ridge area, outwash drained around the sides of the moraine during MIS 2. Nearby sample BN-11-05 dates to 29.7 ± 0.6 ka and may also be part of an older moraine preserved in this area.

6.1.3. MIS 2 and Termination 1 chronology

We date the overall MIS 2 advance to 23.6 ± 0.9 ka. While the mapping identifies a series of at least 6 moraine crests (Fig. 3), the chronology shows that the outermost of these were deposited within a short time frame (i.e. faster than the dating uncertainty; Fig. 2). The more inboard crests are narrow with low relief, likely indicating that the glacier was not sitting in these positions for an extended period. However, smaller recessional moraines within an area dominated by kame terraces (southeast portion of Fig. 2B) date to ~23.5 ka, likely representing close to the final retreat from the moraine complex, and indicate that this sequence of moraines was probably deposited around the same time period within uncertainty.

Towards the center of the left lateral margin of the main sublobe, we mapped what appears to be a breach lobe moraine (Fig. 3A, at samples BN-11-02 and BN-11-01). A moraine can act as a dam for a glacier so that its front builds up until the ice exploits a gap in the ridge, forming an arc-shaped moraine that cross-cuts older moraines (Benn and Evans, 2014). We dated two boulders on this moraine which came out indistinguishable within uncertainty, at 21.7 ± 0.4 and 22.1 ± 0.4 ka.

This chronology shows that the Nirehuao glacier lobe was largest during MIS 2 at 23.6 \pm 0.9 ka (average of both sub-lobes), and in the mapped area may not have had another major, longterm stabilization before the last deglaciation. In the exhaustive mapping of the study area, we did not locate another major margin inboard of Nire 1; however, hugging the paleolake high stand is a thin band of subdued, dissected, inboard-sloping moraine for which we do not have dating control. The Coyhaigue glacier in the next valley to the south reached the innermost MIS 2 maximum after ~21.8 cal ka BP (Miranda, 2015) and before ~17.9 cal ka BP, and then readvanced at ~16.8 cal ka BP (Villa-Martínez and Moreno, 2021). Data from the Río Cisnes valley, just to the north of Nirehuao, show deposition of a recessional moraine at 20.1 \pm 1.2 ka (García et al., 2019). A valuable avenue for future work in the Nirehuao area would be to date moraines that are potentially <23.6 ka, along with lake sediments in the valley to pinpoint glacier withdrawal. Such efforts would also help determine whether glacier stabilizations or advances occurred between ~23.6 and 18.5 ka and resultant landforms were overprinted in a subaqueous setting, and hence there is an apparent lack of moraines.

After ice retreated from the moraine margin, the valley was occupied by an extensive lake in the valley that drained to the Atlantic. The modern drainage of the Río Ñirehuao valley reaches the Pacific via the Río Aysén, but during glacial periods when the valleys to the west were clogged with glaciers, the Ñirehuao glacier lobe, like the Coyhaique/Balmaceda, Lago Buenos Aires, and Pueyrredón lobes (Mercer, 1976) drained to the Atlantic as evidenced by the dry spillway at ~750 masl cut into the southeastern section of Ñire 1 moraines (blue arrow in Fig. 1B). The smaller northern sub-lobe may have hosted a higher elevation lake, as shorelines are preserved up to ~880 masl. Within the mapped area, three hanging channels are incised into the ridge separating the sub-lobes (Fig. 2A) which may have drained the perched lake into the lake of the main sub-lobe.

The major high stands of the Coyhaique/Balmaceda proglacial lake to the south of Ñirehuao (Fig. 1C) reached similar elevations as in Ñirehuao, suggesting that this lake may have been connected to the Ñirehuao deglacial lake. The Coyhaique/Balmaceda proglacial lake had a high stand between 726 and 650 masl dated between ~17.9 and 17.2 cal ka BP and lowered to 650-570 masl at ~17.2—16.2 cal ka BP (Vilanova et al., 2019; Villa-Martínez and Moreno, 2021).

Our youngest MIS 2 ages are congruent with the 18.5 ± 0.2 cal ka BP minimum deglaciation age from Laguna la Trapananda (Weller et al., 2019), which is perched above Valle Richiardi tributary valley (Fig. 1B) at an elevation of 1160 masl. This suggests that the Nirehuao glacier could have been less extensive than its full glacial position by this time, as the Nire 1 moraine is at a lower elevation (the average elevation of the boulders from the Nire 1 moraine is 915 masl). Laguna La Trapananda sits on a plateau above Valle Richiardi, and so it does not indicate that the glacier had retreated beyond this margin, but rather that it had thinned below 1160 masl by this time.

6.2. The Nirehuao record in the broader climate context

6.2.1. Pre MIS 6

The single age from the farthest outboard, highest elevation moraine crest in the study area falls squarely within MIS 8, and overlaps within uncertainty with the MIS 8 glacial maximum conditions of temperature and dust flux in Antarctica (Fig. 9E and F). Albeit just one age, it is identical within dating uncertainty to the outwash gravel ages (Fig. 9B; Hein et al., 2009) associated with advances of two glacial lobes around Lago Buenos Aires to the southeast (Fig. 1). Hence, we argue this age is supportive of an MIS 8 Patagonian glaciation, although specifically at Nirehuao it needs confirmation.

6.2.2. MIS 6 and pre-MIS 2

This new record represents one of the first studies to directly date a MIS 6 advance of the Patagonian Ice Sheet and show that it was more extensive than during MIS 2. In many paleoclimate records (e.g. benthic δ^{18} O, Antarctic temperature, dust flux, Fig. 9), MIS 6 is the last time that climate conditions reached MIS 2 levels. In this sense, the Nirehuao record is concordant with regional/global climate records and the lack of other direct dating of MIS 6 in Patagonia may largely represent a gap in the application of exposure dating to pre-MIS 2 moraines. However studies from Lago Buenos Aires and Lago Pueyrredón have reported ages from the deposits outboard of the MIS 2 moraines dating to MIS 8 (Hein et al., 2009, 2017), meaning that these two glacier lobes were probably similar in size or more extensive during MIS 2 than during MIS 6.

The Nirehuao lobe likely expanded twice during MIS 6, at ~153 ka and ~137 ka (vertical gray bars in Fig. 9). This bimodal MIS 6 is paralleled by Antarctic temperature (Fig. 9E; Parrenin et al., 2013), dust flux (Fig. 9F; Lambert et al., 2012), and sea salt sodium flux (Fig. 9G; Wolff et al., 2006), in which peak glacial conditions are

reached twice, punctuated by a reprieve at ~150 ka. The U^K₃₇ sea surface temperature (SST) record of de Bar et al. (2018) appears to also reflect this bimodality, but the record ends around this time (Fig. 9D). Notably, this pattern is attenuated or absent in the more globally representative LR04 stack (Fig. 9C; Lisiecki and Raymo, 2005). Altogether, this suggests that in the southern hemisphere, MIS 6, similar to MIS 2, had internal structure with multiple episodes of peak glacial conditions.

Three marine cores offshore of western Patagonia around a similar latitude to Ñirehuao extend into MIS 6, ODP 1234 (Fig. 9D; 36°S; extends to 150 ka; de Bar et al., 2018), GeoB 3327–5 (43°S; extends to ~500 ka) and PS75/034–2 (54°S; extends to ~700 ka; Ho et al., 2012). U^K₃₇ SST reconstructions at all three sites show MIS 6 cooling more similar to average interglacial conditions than to conditions during MIS 2 or 4. Further study on MIS 6 is needed to resolve this potential discrepancy between our extensive MIS 6 glaciation on land and mild offshore conditions, including any potential connection to the build-up of the Patagonian Ice Sheet (e.g., Mendelová et al., 2020).

Interestingly, we found no evidence for a more extensive glaciation during MIS 4 than at MIS 2, which is prominent at the southern tip of the continent (Fig. 9B; Peltier et al., 2021), in New Zealand (Schaefer et al., 2015), and elsewhere around the globe (Doughty et al., 2021). Indirect evidence exists to the west of Nirehuao in the Chilean Lake District, where Heusser et al. (2000) inferred that the MIS 4 glacier limits were the most extensive of the last glacial cycle based on a bog record. It is possible at Nirehuao that the MIS 4 and 2 glaciations were similar in extent, with the latter slightly more extensive.

Additional ages are needed to ascertain whether BN-18-102 $(42.0 \pm 0.8 \text{ ka})$ is a minimum age or accurately reflects a small preserved ice marginal landform. We note that García et al. (2018) dated moraines to the south, at Torres del Paine National Park (51°S, 72°W, 650 km south of Nirehuao) to 47.8 \pm 2.3 ka, although these ice-marginal landforms show glaciers were much more extensive than during MIS 2. At Nirehuao on the other hand, a potential MIS 3 advance (i.e. the moraine with one age of 42.0 ± 0.8 ka) would have extended nearly the same distance as during MIS 2. In the Chilean Lake District, ~300 km to the northwest, expansions of the Patagonian ice sheet occurred between ~34 and 18 cal ka BP (Moreno et al., 2015). However, the most extensive advances were between ~27 and 18 cal ka BP, and prior advances <34 cal ka BP are preserved in stratigraphic-based evidence. We also note that major MIS 3 advances have been identified in New Zealand (Kelley et al., 2014; Doughty et al., 2015; Strand et al., 2019). Overall, the Ñirehuao record offers valuable insight into MIS 6 but more work is needed on the period between MIS 6 and 2.

6.2.3. MIS 2 and Termination 1

The Nire 1 moraine mean of 23.6 \pm 0.9 ka may reflect the end of Southern Hemisphere peak MIS 2 cooling. The peak MIS 2 Antarctic temperature and dust flux (Parrenin et al., 2013; Lambert et al., 2012) occurs between ~26.5-24.5 ka and was followed by a small pulse of warming (Fig. 9). Local offshore marine records also have pronounced mid-MIS 2 minima between ~27-24 ka in SST, e.g. ODP 1234 (Fig. 9D; 36°S; de Bar et al., 2018), ODP 1233 (41°S; Kaiser and Lamy, 2010), and in the planktonic foraminiferal fauna record from TNO57-21 (41°S; Barker and Diz, 2014). (In contrast, alkenone SSTs in core MD07-3128 (53°S; Caniupán et al., 2011) cool through MIS 2 similar to the trend in the LR04 benthic stack (Fig. 9C)). Furthermore, cosmogenically-dated MIS 2 moraine records from Patagonia (e.g., Kaplan et al., 2004; Douglass et al., 2006; Hein et al., 2010; Mendelová et al., 2020; Peltier et al., 2021), along with ¹⁴C-dated records in the Chilean Lake District (e.g., Moreno et al., 2015), generally cluster into two groups, one group between ~28 and 24 ka

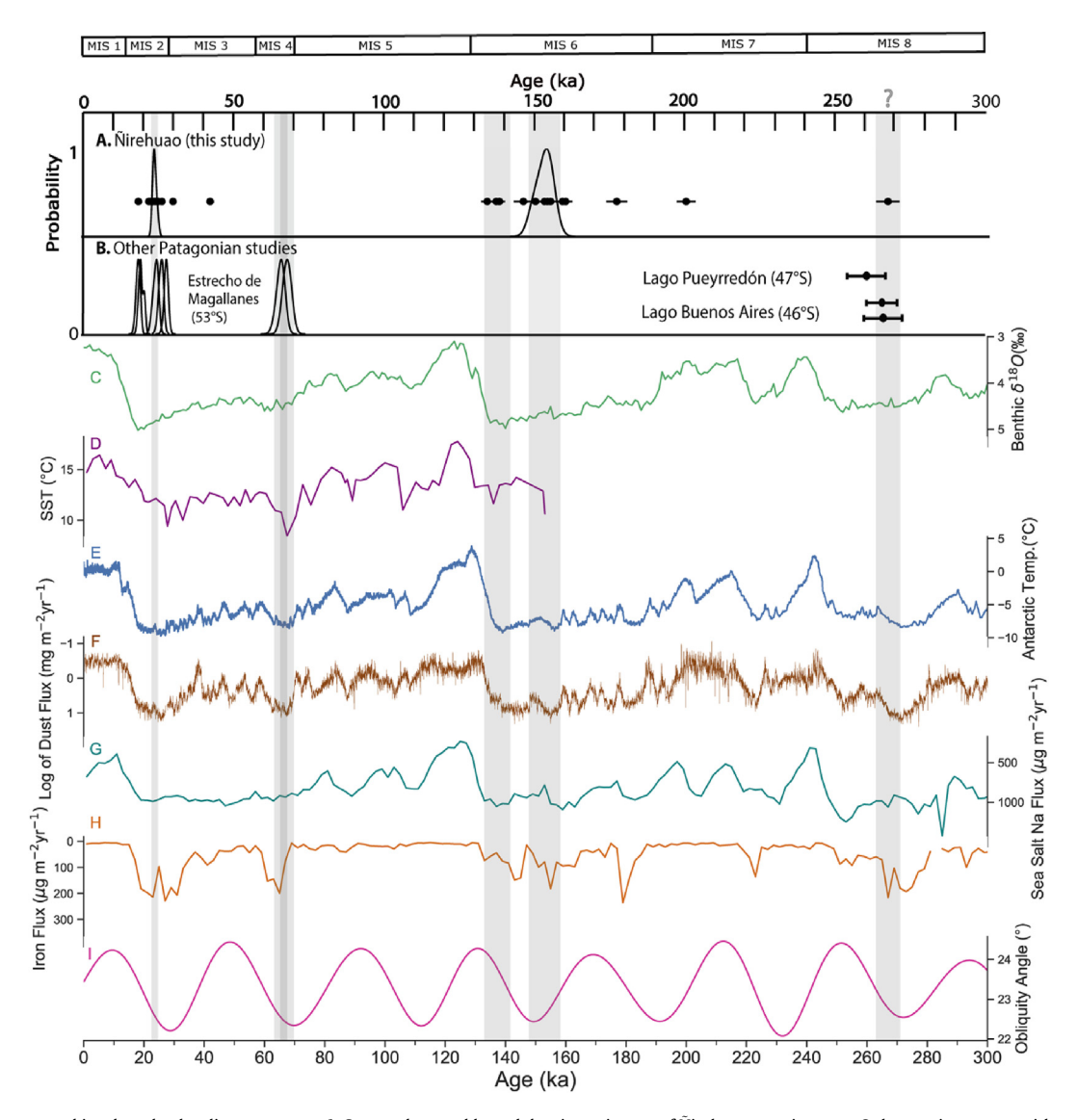


Fig. 9. The Nirehuao record in a broad paleoclimate context. **A.** Summed normal kernel density estimates of Nirehuao moraine ages. Only moraine means with more than two ages are plotted as normal kernel density estimates. Vertical gray bars represent the 1 σ bounds for the moraine averages (3% production rate uncertainty included), with the MIS 4 moraine averages from Estrecho de Magallanes also displayed as a gray bar. The gray bar at ~270 ka is based on only one age and so we mark it with a question mark. Black dots show all individual samples. **B.** Other terrestrial Patagonian studies (locations of which are shown in Fig. 1A). Summed normal kernel density estimates from Estrecho de Magallanes moraines with individual samples plotted as thin curves. Lago Pueyrredón and Lago Buenos Aires outwash terrace ages from Hein et al. (2009). **C.** The LR04 benthic δ^{18} O stack from Lisiecki and Raymo (2005). **D.** U^K₃₇ based seawater surface temperature record from ODP 1234 (36°S; de Bar et al., 2018). **E.** Antarctic temperature stack from 5 ice cores (Parrenin et al., 2013). **F.** Natural logarithm of the dust flux from EPICA Dome C (Lambert et al., 2012). **G.** Sea salt sodium flux and **H.** Iron flux from the Dome C Antarctic ice core (Wolff et al., 2006). **I.** Obliquity angle from Laskar et al. (2004).

and another between ~21 and 18 ka, where the gap between coincides with the small peak in Antarctic dust and temperature. The New Zealand record also lacks dated moraines during the middle of MIS 2, as glaciers there were largest before, at ~29-27 ka, and readvanced after, at ~21-18 ka, with a notable lack of moraines during Heinrich stadial 2 (~26–23.5 ka). This gap in the moraine sequence may also correspond to the beginning of the Varas interstade (Mercer, 1976), identified in pollen records from northwestern Patagonia occurring at ~25-19.2 cal ka BP (Moreno et al., 2015, 2018). We propose that the Nirehuao MIS 2 maximum, at 23.6 ± 0.9 ka, overlapping with the Estrecho de Magallanes 23.9 ± 0.8 ka moraine (Peltier et al., 2021), represents the end of the peak MIS 2 coldest conditions over Antarctica, and the start of interstadial conditions (potentially the Varas interstadial) causing the Nirehuao glacier lobe to start to pull back from its MIS 2 maximum margin.

Our ages from the inner moraines in the area signify that the glacier was large and stable until at least 24.1 \pm 0.8 ka (n = 3), representing a maximum-limiting age for Termination 1 (but not necessarily a close maximum estimate). Our radiocarbon-dated onset of organic lake sedimentation in Lago Mano Negra (Fig. 1B; 840 masl) indicates local ice-free conditions at ~18.5 ka, approximately 300 m above the Río Emperador Guillermo valley floor and ~42 km upstream from the Nire 1 moraines, affording a minimum limiting age estimate for the deposition of those moraines and cessation of local ice-dammed conditions. The statistically indistinguishable basal age of 18.5 \pm 0.2 cal ka BP from Laguna La Trapananda (Weller et al., 2019), located ~12.5 km downstream along the glacier flowline and ~300 m higher elevation than Lago Mano Negra, suggest that thinning and recession of the southernmost tributary glacier of the Nirehuao lobe exposed this valley within the LGM, and indicate that the earliest phase of glaciolacustrine

flooding of the Nirehuao valley and Valle Emperador Guillermo (>840 masl) was a short-lived event.

Sea salt sodium flux in the Dome C Antarctic ice core is thought to be a proxy for winter sea ice extent, where flux is higher in colder conditions because of new sea-ice formation (Wolff et al., 2006). Extensive sea ice around Antarctica would be associated with colder climates farther north towards southern South America (Gersonde et al., 2005) and likely helps to link the middle and higher latitudes through its connection to Southern Ocean stratification (Sigman and Haug, 2003; Putnam et al., 2010). Indeed, Putnam et al. (2010) suggested a link between sea ice in the Southern Ocean and the Ohau glacier record in New Zealand, where they propose that sea-ice expansion caused by high latitude winter cooling and increasing winter duration (Huybers and Denton, 2008) promoted Southern Ocean stratification which cooled the surrounding regions during the Ohau local LGM. Sea salt sodium flux in the Dome C core (Wolff et al., 2006) suggests sea ice was more extensive from MIS 2 through MIS 4, while the Estrecho de Magallanes record similarly shows that the lobe was large during MIS 4, potentially MIS 3, and early on in MIS 2 (Peltier et al., 2021). Sea salt sodium flux also suggests sea ice was more extensive during MIS 8 than MIS 6, and more extensive during MIS 6 than during MIS 2, also with a two-peak MIS 6. The Nirehuao record shows this same relative extent for the glacier lobe, potentially reflecting a parallel evolution of sea ice extent and the extent of the Patagonian Ice Sheet at the glacial timescale, suggesting that winter sea ice extent and Southern Ocean stratification could help link climate in Patagonia to the higher latitudes during glacial periods.

Similar to the Estrecho de Magallanes record, the timing of glacial maxima in Ñirehuao has little in common with local summer insolation intensity (Fig. 10). Insolation intensity at 45°S (Laskar et al., 2004) reaches a minimum during MIS 6 at 175 ka, and fluctuates between intermediate levels from 135 to 160 ka. Meanwhile, obliquity reaches a minimum at 150 ka, in line with the Ñirehuao MIS 6. The following minimum in obliquity at 191 ka coincides with

the pre-MIS 6 age of 192 \pm 15 ka (Table 2; n = 3), although we note the large scatter in this age group may indicate this is a minimum age. The following minimum in obliquity occurs during MIS 7, when sea salt sodium flux indicates that sea ice extent may have been low. The next minimum occurs at 273 ka (Laskar et al., 2004), consistent with the single MIS 8 age (267 \pm 8.9 ka), especially considering it is likely a minimum age.

Iron in Antarctic cores almost exclusively comes from terrestrial dust sources (Wolff et al., 2006), and the main source of dust is thought to be Patagonia (e.g. Basile et al., 1997; Sugden et al., 2009; Gili et al., 2016, 2017). The major minima in iron flux (Fig. 9H) appear to be spaced about 40 kyr apart, with a gap during MIS 5. Iron flux maxima occur when obliquity angle increases to about 22.5°, i.e. about 5 kyr after the obliquity minima. Iron flux minima also occur when the Estrecho de Magallanes lobe was largest, clustering toward the beginning and end of MIS 2, and around 65 ka. Beyond MIS 4, we see two iron peaks during MIS 6, similar to the Ñirehuao record, and potentially a match between the three single 10 Be ages and iron peaks between MIS 6 and MIS 8, and during MIS 8 (n = 1). Thus, iron flux at Dome C appears to be consistent with the Nirehuao glacier records, and also appears to contain a strong periodicity on the obliquity timescale, suggesting a potential link between glaciations in Patagonia, dustiness over Antarctica, and the obliquity cycle. We propose that the climate systems that mediate the relationship between insolation and glacier extent in Patagonia are particularly sensitive to earth's obliquity cycle (cf., Doughty et al., 2021; Huybers and Denton, 2008).

Glacial maxima occur in Patagonia when sea ice around Antarctica is extensive, and eccentricity and obliquity reach minima. Taken together, the climate in Antarctica and Patagonia may be in closer communication during glacial periods; the Subantarctic front shifts north, closer to Patagonia, which sends more dust to Antarctica. More extensive sea ice and Southern Ocean stratification likely help bring colder climates to Patagonia, and may set the stage for the Patagonian Ice Sheet, and the glaciers in

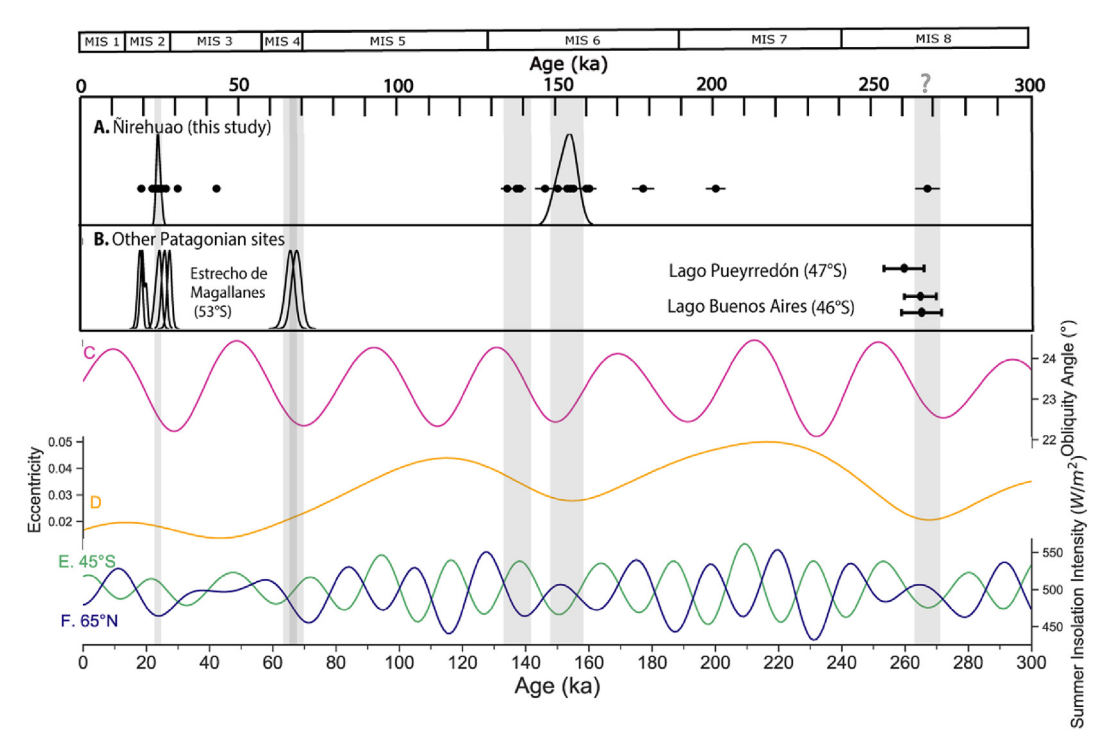


Fig. 10. The Nirehuao record and orbital parameters. Panels A—B and vertical gray bars are identical to those in Fig. 9. C. Obliquity angle. D. Eccentricity. E. December 21st insolation intensity at 45°S. F. June 21st insolation intensity at 65°N. Data on panels C—F are from Laskar et al. (2004).

New Zealand (Putnam et al., 2010), to expand.

7. Conclusions

The Ñirehuao glacier valley records a long sequence of successive glacier advances that we map and date to MIS 2, MIS 6 and potentially MIS 8, representing the first detailed glacial chronology for the Ñirehuao glacier lobe and direct dating of a MIS 6 glacial advance in Patagonia. We found that two neighboring sub-lobes converged near their terminal margin and produced identical glacier chronologies within error. We also present the highest resolution geomorphic map of the Ñirehuao glacier maxima to date. This work details an example of a more complicated geometry between the existing bedrock and the ice sheet at the margins of more than one glacier sub-lobe, which hopefully will help others interpret glacial lobe geometries at similar sites in the future.

Altogether this new chronology and mapping show that in the Nirehuao glacier valley:

- A major, moraine-forming advance may have occurred by 267 ± 8.9 ka, in line with better dated records in central Patagonia, during MIS 8, and potentially between MIS 6 and 8.
- The lobe likely reached a maximum at least twice during MIS 6. The lobe formed a major set of moraines by 153 ± 5.1 ka, and likely expanded again by 137 ± 4.2 ka. These two time periods correspond with the two coldest and dustiest periods of MIS 6 in Antarctica. This dataset represents one of the first directly dated records of a MIS 6 glacier advance in Patagonia.
- The lobe reached its maximum extent during MIS 2 at 23.6 ± 0.9 ka, at the end of peak MIS 2 cooling in the southern hemisphere. Currently there is no dated moraine evidence in this valley of another major readvance during MIS 2. This age represents a maximum limiting age for the start of Termination 1, and further work is necessary to more closely constrain the timing of Termination 1 at this site.
- Subsequently, retreat of the glacier commenced by ~18.5 cal ka BP when two lakes in a tributary valley just to the southwest became ice-free. A large ice-dammed lake formed in the Nirehuao and adjacent valleys during Termination 1.
- Overall, the timing of glacial culminations in Patagonia tends to correspond with times when winter sea ice is expansive and both obliquity and eccentricity are at minima. We do not find evidence for extensive glaciation at times when obliquity is low but eccentricity is high, or at times when eccentricity is low but obliquity is high.

Credit author statement

Carly Peltier: Data collection and analysis, wrote the paper with contributions from all coauthors. Michael Kaplan: Conceived and designed the project, collected and contributed data. Esteban A. Sagredo: Contributed to data collection and analysis. Patricio I. Moreno: Contributed to data collection and analysis. José Araos: Contributed to data collection. Sean D. Birkel: Contributed to data analysis. Rodrigo Villa-Martinez: Contributed to data collection and analysis. Roseanne Schwartz: Designed and contributed to data analysis. Scott Reynhout: Contributed to data collection and analysis. Joerg M. Schaefer: Conceived and designed the analysis.

Funding

This work was supported by the National Science Foundation, NSF-BCS #1263474 (Kaplan, Schaefer) and #1263574 (Birkel), and the LDEO and NASA GISS Climate Center. This work was also

supported by funding from FONDECYT 1180815 and 1121141 (Villa-Martínez) and ANID/BASAL FB210018 (Villa-Martínez). We also acknowledge the Fulbright Commission Visiting Scholar Grant (Kaplan), and Fulbright U.S. Student Grant (Peltier).

Declaration of competing interest

The authors declare that they have no known competing financial interests or personal relationships that could have appeared to influence the work reported in this paper.

Data availability

Data will be made available on request.

Acknowledgments

We would like to thank Isabel Vilanova, Tomás Marín, and Sebastian Felipe Ruiz Pereira for their help in the field with sample collection, and Jeremy Frisch and Jean Hanley for their help processing samples. We also thank Jerry McManus and Sidney Hemming for their feedback on the project, and Gordon Bromley and an anonymous Reviewer.

References

- Abe-Ouchi, A., Saito, F., Kawamura, K., Raymo, M.E., Okuno, J., Takahashi, K., Blatter, H., 2013. Insolation-driven 100,000-year glacial cycles and hysteresis of ice-sheet volume. Nature 500, 190—193. https://doi.org/10.1038/nature12374.
- Applegate, P.J., Urban, N.M., Laabs, B.J., Keller, K., Alley, R.B., 2010. Modeling the statistical distributions of cosmogenic exposure dates from moraines. Geosci. Model Dev. (GMD) 3 (1), 293–307.
- Balco, G., Stone, J.O., Lifton, N.A., Dunai, T.J., 2008. A complete and easily accessible means of calculating surface exposure ages or erosion rates from ¹⁰Be and ²⁶Al measurements. Quaternary Geochronology, Prospects for the New Frontiers of earth and Environmental Sciences 3, 174–195. https://doi.org/10.1016/j.quageo.2007.12.001.
- Barker, S., Diz, P., 2014. Timing of the descent into the last Ice Age determined by the bipolar seesaw. Paleoceanography 29, 489–507. https://doi.org/10.1002/ 2014PA002623.
- Basile, I., Grousset, F.E., Revel, M., Petit, J.R., Biscaye, P.E., Barkov, N.I., 1997. Patagonian origin of glacial dust deposited in East Antarctica (Vostok and Dome C) during glacial stages 2, 4 and 6. Earth Planet Sci. Lett. 146, 573–589. https://doi.org/10.1016/S0012-821X(96)00255-5.
- Bendle, J.M., Thorndycraft, V.R., Palmer, A.P., 2017. The glacial geomorphology of the lago Buenos Aires and lago Pueyrredón ice lobes of central Patagonia. J. Maps 13, 654–673. https://doi.org/10.1080/17445647.2017.1351908.
- Benn, D., Evans, D.J.A., 2014. Glaciers and Glaciation, second ed. Routledge.
- Caldenius, C.C., 1932. Las Glaciaciones Cuaternarias en la Patagonia y Tierra del Fuego. Geogr. Ann. 14, 1–164. https://doi.org/10.1080/20014422.1932.11880545.
- Caniupán, M., Lamy, F., Lange, C.B., Kaiser, J., Arz, H., Kilian, R., Baeza Urrea, O., Aracena, C., Hebbeln, D., Kissel, C., Laj, C., Mollenhauer, G., Tiedemann, R., 2011. Millennial-scale sea surface temperature and Patagonian Ice Sheet changes off southernmost Chile (53°S) over the past -60 kyr: SST changes off southern Chile. Paleoceanography 26. https://doi.org/10.1029/2010PA002049.
- Clapperton, C.M., 1993. Quaternary Geology and Geomorphology of South America. Elsevier Science Publishers B. V, Amsterdam.
- Clark, P.U., Dyke, A.S., Shakun, J.D., Carlson, A.E., Clark, J., Wohlfarth, B., Mitrovica, J.X., Hostetler, S.W., McCabe, A.M., 2009. The last glacial maximum. Science 325 (5941), 710e714.
- Cogez, A., Herman, F., Pelt, É., Reuschlé, T., Morvan, G., Darvill, C.M., Norton, K.P., Christl, M., Märki, L., Chabaux, F., 2018. U–Th and ¹⁰Be constraints on sediment recycling in proglacial settings, Lago Buenos Aires, Patagonia. Earth Surf. Dyn. 6, 121–140. https://doi.org/10.5194/esurf-6-121-2018.
- 121–140. https://doi.org/10.5194/esurf-6-121-2018. Cooper, E.L., Thorndycraft, V.R., Davies, B.J., Palmer, A.P., García, J.L., 2021. Glacial geomorphology of the former patagonian ice sheet (44–46° S). J. Maps 17 (2), 661–681.
- Coronato, A., Martínez, O., Rabassa, J., 2004. Glaciations in Argentine Patagonia, southern South America. In: Ehlers, J., Gibbard, P.L. (Eds.), Developments in Quaternary Sciences, Quaternary Glaciations Extent and Chronology. Elsevier, pp. 49–67. https://doi.org/10.1016/S1571-0866(04)80111-8.
- Darvill, C.M., Bentley, M.J., Stokes, C.R., Hein, A.S., Rodés, Á., 2015. Extensive MIS 3 glaciation in southernmost Patagonia revealed by cosmogenic nuclide dating of outwash sediments. Earth Planet Sci. Lett. 429, 157–169.
- Darvill, C.M., Bentley, M.J., Stokes, C.R., Shulmeister, J., 2016. The timing and cause of glacial advances in the southern mid-latitudes during the last glacial cycle based on a synthesis of exposure ages from Patagonia and New Zealand. Quat.

- Sci. Rev. 149, 200-214. https://doi.org/10.1016/j.quascirev.2016.07.024.
- Darvill, C.M., Stokes, C.R., Bentley, M.J., Evans, D.J.A., Lovell, H., 2017. Dynamics of former ice lobes of the southernmost Patagonian Ice Sheet based on a glacial landsystems approach. J. Quat. Sci. 32, 857–876. https://doi.org/10.1002/ ins.2890
- Darvill, C.M., Stokes, C.R., Bentley, M.J., Lovell, H., 2014. A glacial geomorphological map of the southernmost ice lobes of Patagonia: the bahía inútil san sebastián, magellan, otway, skyring and Río gallegos lobes. J. Maps 10, 500—520. https://doi.org/10.1080/17445647.2014.890134.
- Davies, B.J., Darvill, C.M., Lovell, H., Bendle, J.M., Dowdeswell, J.A., Fabel, D., García, J.-L., Geiger, A., Glasser, N.F., Gheorghiu, D.M., Harrison, S., Hein, A.S., Kaplan, M.R., Martin, J.R.V., Mendelova, M., Palmer, A., Pelto, M., Rodés, Á., Sagredo, E.A., Smedley, R.K., Smellie, J.L., Thorndycraft, V.R., 2020. The evolution of the Patagonian Ice Sheet from 35 ka to the present day (PATICE). Earth Sci. Rev. 204, 103152. https://doi.org/10.1016/j.earscirev.2020.103152.
- de Bar, M.W., Stolwijk, D.J., McManus, J.F., Sinninghe Damsté, J.S., Schouten, S., 2018. A Late Quaternary climate record based on long-chain diol proxies from the Chilean margin. Clim. Past 14, 1783–1803. https://doi.org/10.5194/cp-14-1783-2018
- Doughty, A.M., Kaplan, M.R., Peltier, C., Barker, S., 2021. A maximum in global glacier extent during MIS 4. Quat. Sci. Rev. 261, 106948. https://doi.org/10.1016/ i.guascirev.2021.106948.
- Doughty, A.M., Schaefer, J.M., Putnam, A.E., Denton, G.H., Kaplan, M.R., Barrell, D.J.A., Andersen, B.G., Kelley, S.E., Finkel, R.C., Schwartz, R., 2015. Mismatch of glacier extent and summer insolation in Southern Hemisphere mid-latitudes. Geology 43. 407–410. https://doi.org/10.1130/G36477.1.
- Douglass, D.C., Singer, B.S., Ackert, M.R., Kaplan, M.R., Caffee, M.W., 2007. Constraining boulder erosion rates and ages of mid-Pleistocene moraines Lago Buenos Aires, Argentina. GSA Abstracts and Programs Northeastern Section, 42nd Annual Meeting.
- Douglass, D.C., Singer, B.S., Kaplan, M.R., Mickelson, D.M., Caffee, M.W., 2006. Cosmogenic nuclide surface exposure dating of boulders on last-glacial and late-glacial moraines, Lago Buenos Aires, Argentina: interpretive strategies and paleoclimate implications. Quaternary Geochronology, Terrestrial Cosmogenic Nuclides 1, 43–58. https://doi.org/10.1016/j.quageo.2006.06.001.
- García, J.-L., Hall, B.L., Kaplan, M.R., Vega, R.M., Strelin, J.A., 2014. Glacial geomorphology of the Torres del Paine region (southern Patagonia): implications for glaciation, deglaciation and paleolake history. Geomorphology 204, 599–616. https://doi.org/10.1016/j.geomorph.2013.08.036.
- García, J.-L., Hein, A.S., Binnie, S.A., Gómez, G.A., González, M.A., Dunai, T.J., 2018. The MIS 3 maximum of the Torres del Paine and Última Esperanza ice lobes in Patagonia and the pacing of southern mountain glaciation. Quat. Sci. Rev. 185, 9–26. https://doi.org/10.1016/j.quascirev.2018.01.013.
- García, J.-L., Maldonado, A., de Porras, M.E., Nuevo Delaunay, A., Reyes, O., Ebensperger, C.A., Binnie, S.A., Lüthgens, C., Méndez, C., 2019. Early deglaciation and paleolake history of Río Cisnes glacier, patagonian ice sheet (44°S). Quat. Res. (Orlando) 91, 194–217. https://doi.org/10.1017/qua.2018.93.
- Garreaud, R.D., Vuille, M., Compagnucci, R., Marengo, J., 2009. Present-day south American climate. Palaeogeography, Palaeoclimatology, Palaeoecology, Longterm multi-proxy climate reconstructions and dynamics in South America (LOTRED-SA): State of the art and perspectives 281 180–195. https://doi.org/ 10.1016/j.palaeo.2007.10.032.
- Gersonde, R., Crosta, X., Abelmann, A., Armand, L., 2005. Sea-surface temperature and sea ice distribution of the Southern Ocean at the EPILOG Last Glacial Maximum—a circum-Antarctic view based on siliceous microfossil records. Quaternary Science Reviews, Multiproxy Approach for the Reconstruction of the Glacial Ocean surface 24, 869–896. https://doi.org/10.1016/j.quascirev.2004.07.015.
- Gili, S., Gaiero, D.M., Goldstein, S.L., Chemale, F., Jweda, J., Kaplan, M.R., Becchio, R.A., Koester, E., 2017. Glacial/interglacial changes of Southern Hemisphere wind circulation from the geochemistry of South American dust. Earth Planet Sci. Lett. 469, 98–109. https://doi.org/10.1016/j.epsl.2017.04.007.
- Gili, S., Gaiero, D.M., Goldstein, S.L., Chemale Jr., F., Koester, E., Jweda, J., Vallelonga, P., Kaplan, M.R., 2016. Provenance of dust to Antarctica: a lead isotopic perspective: PB Isotopic signature in Antarctic Dust. Geophys. Res. Lett. 43, 2291–2298. https://doi.org/10.1002/2016GL068244.
- Gillespie, A.R., Bierman, P.R., 1995. Precision of terrestrial exposure ages and erosion rates estimated from analysis of cosmogenic isotopes produced in situ. J. Geophys. Res. Solid Earth 100, 24637–24649. https://doi.org/10.1029/ 95JB02911.
- Glasser, N., Jansson, K., 2008. The glacial map of southern South America. J. Maps 4, 175–196. https://doi.org/10.4113/jom.2008.1020.
- Glasser, N.F., Jansson, K.N., Duller, G.A.T., Singarayer, J., Holloway, M., Harrison, S., 2016. Glacial lake drainage in Patagonia (13-8 kyr) and response of the adjacent Pacific Ocean. Sci. Rep. 6, 21064. https://doi.org/10.1038/srep21064.
- Glasser, N.F., Jansson, K.N., Harrison, S., Kleman, J., 2008. The glacial geomorphology and Pleistocene history of South America between 38°S and 56°S. Quat. Sci. Rev. 27, 365–390. https://doi.org/10.1016/j.quascirev.2007.11.011.
- Hays, J.D., Imbrie, J., Shackleton, N.J., 1976. Variations in the Earth's Orbit: Pacemaker of the Ice Ages 194, p. 13.
- Hein, A.S., Cogez, A., Darvill, C.M., Mendelova, M., Kaplan, M.R., Herman, F., Dunai, T.J., Norton, K., Xu, S., Christl, M., Rodés, A., 2017. Regional mid-Pleistocene glaciation in central Patagonia. Quat. Sci. Rev. 164, 77–94. https:// doi.org/10.1016/j.quascirev.2017.03.023.
- Hein, A.S., Dunai, T.J., Hulton, N.R.J., Xu, S., 2011. Exposure dating outwash gravels to

- determine the age of the greatest Patagonian glaciations. Geology 39, 103–106. https://doi.org/10.1130/G31215.1.
- Hein, A.S., Hulton, N.R.J., Dunai, T.J., Schnabel, C., Kaplan, M.R., Naylor, M., Xu, S., 2009. Middle Pleistocene glaciation in Patagonia dated by cosmogenic-nuclide measurements on outwash gravels. Earth Planet Sci. Lett. 286, 184–197. https://doi.org/10.1016/j.epsl.2009.06.026.
- Hein, A.S., Hulton, N.R.J., Dunai, T.J., Sugden, D.E., Kaplan, M.R., Xu, S., 2010. The chronology of the Last Glacial Maximum and deglacial events in central Argentine Patagonia. Quat. Sci. Rev. 29, 1212–1227. https://doi.org/10.1016/ i.quascirev.2010.01.020.
- Hepp, C., Reyes, C., Muñoz, R., 2018. Análisis de dato históricos de cinco estaciones meteorológicas de la región de Aysén (Patagonia).
- Heusser, C.J., Lowell, T.V., Heusser, L.E., 2000. Pollen sequence from the Chilean Lake District during the Llanquihue glaciation in marine oxygen isotope stages 4–2. J. Quat. Sci.: Published for the Quaternary Research Association 15 (2), 115–125.
- Heyman, J., Stroeven, A.P., Harbor, J.M., Caffee, M.W., 2011. Too young or too old: evaluating cosmogenic exposure dating based on an analysis of compiled boulder exposure ages. Earth Planet Sci. Lett. 302, 71–80. https://doi.org/10.1016/j.epsl.2010.11.040.
- Heyman, J., Applegate, P.J., Blomdin, R., Gribenski, N., Harbor, J.M., Stroeven, A.P., 2016. Boulder height—exposure age relationships from a global glacial 10Be compilation. Quat. Geochronol. 34, 1–11.
- Ho, S.L., Mollenhauer, G., Lamy, F., Martínez-Garcia, A., Mohtadi, M., Gersonde, R., Hebbeln, D., Nunez-Ricardo, S., Rosell-Melé, A., Tiedemann, R., 2012. Sea surface temperature variability in the Pacific sector of the Southern Ocean over the past 700 kyr: the 700 kyr south pacific SST variability. Paleoceanography 27. https:// doi.org/10.1029/2012PA002317.
- Hughes, P.D., Gibbard, P.L., Ehlers, J., 2013. Timing of glaciation during the last glacial cycle: evaluating the concept of a global 'Last Glacial Maximum' (LGM). Earth Sci. Rev. 125, 171–198.
- Huybers, P., Denton, G., 2008. Antarctic temperature at orbital timescales controlled by local summer duration. Nat. Geosci. 1, 787–792. https://doi.org/10.1038/ngeo311.
- Imbrie, J., Boyle, E.A., Clemens, S.C., Duffy, A., Howard, W.R., Kukla, G., Kutzbach, J., Martinson, D.G., McIntyre, A., Mix, A.C., Molfino, B., Morley, J.J., Peterson, L.C., Pisias, N.G., Prell, W.L., Raymo, M.E., Shackleton, N.J., Toggweiler, J.R., 1992. On the structure and origin of major glaciation cycles 1. Linear responses to milankovitch forcing. Paleoceanography 7, 701–738. https://doi.org/10.1029/92PA02253.
- Kaiser, J., Lamy, F., 2010. Links between Patagonian Ice Sheet fluctuations and Antarctic dust variability during the last glacial period (MIS 4-2). Quat. Sci. Rev. 29, 1464–1471. https://doi.org/10.1016/j.quascirev.2010.03.005.
- Kaplan, M.R., Ackert Jr., R.P., Singer, B.S., Douglass, D.C., Kurz, M.D., 2004. Cosmogenic nuclide chronology of millennial-scale glacial advances during O-isotope stage 2 in Patagonia. GSA Bulletin 116, 308–321. https://doi.org/10.1130/B25178.1.
- Kaplan, M.R., Douglass, D.C., Singer, B.S., Ackert, R.P., Caffee, M.W., 2005. Cosmogenic nuclide chronology of pre-last glacial maximum moraines at Lago Buenos Aires, 46°S, Argentina. Quat. Res. (Orlando) 63, 301–315. https://doi.org/10.1016/j.yqres.2004.12.003.
- Kaplan, M.R., Strelin, J.A., Schaefer, J.M., Denton, G.H., Finkel, R.C., Schwartz, R., Putnam, A.E., Vandergoes, M.J., Goehring, B.M., Travis, S.G., 2011. In-situ cosmogenic ¹⁰Be production rate at Lago Argentino, Patagonia: implications for late-glacial climate chronology. Earth Planet Sci. Lett. 309, 21–32. https://doi.org/10.1016/j.epsl.2011.06.018.
- Kelley, S.E., Kaplan, M.R., Schaefer, J.M., Andersen, B.G., Barrell, D.J.A., Putnam, A.E., Denton, G.H., Schwartz, R., Finkel, R.C., Doughty, A.M., 2014. High-precision ¹⁰Be chronology of moraines in the Southern Alps indicates synchronous cooling in Antarctica and New Zealand 42,000 years ago. Earth Planet Sci. Lett. 405, 194–206. https://doi.org/10.1016/j.epsl.2014.07.031.
- Lal, D., 1991. Cosmic ray labeling of erosion surfaces: in situ nuclide production rates and erosion models. Earth Planet Sci. Lett. 104, 424–439. https://doi.org/ 10.1016/0012-821X(91)90220-C.
- Lambert, F., Bigler, M., Steffensen, J.P., Hutterli, M., Fischer, H., 2012. Centennial mineral dust variability in high-resolution ice core data from Dome C, Antarctica. Clim. Past 8, 609–623. https://doi.org/10.5194/cp-8-609-2012.
- Laskar, J., Robutel, P., Joutel, F., Gastineau, M., Correia, A.C.M., Levrard, B., 2004. A long-term numerical solution for the insolation quantities of the Earth. Al\&A 428, 261–285. https://doi.org/10.1051/0004-6361:20041335.
- Leger, T.P.M., Hein, A.S., Bingham, R.G., Martini, M.A., Soteres, R.L., Sagredo, E.A., Martínez, O.A., 2020. The glacial geomorphology of the Río corcovado, Río huemul and lago palena/general vintter valleys, northeastern Patagonia (43°S, 71°W). Journal of Maps 16, 651–668. https://doi.org/10.1080/17445647.2020.1794990.
- Leger, T.P., Hein, A.S., Bingham, R.G., Rodés, Á., Fabel, D., Smedley, R.K., 2021. Geomorphology and 10Be chronology of the last glacial maximum and deglaciation in northeastern Patagonia, 43° S-71° W. Quaternary Science Reviews 272, 107194
- Lifton, N., Sato, T., Dunai, T.J., 2014. Scaling in situ cosmogenic nuclide production rates using analytical approximations to atmospheric cosmic-ray fluxes. Earth and Planetary Science Letters 386, 149–160. https://doi.org/10.1016/j.epsl.2013.10.052.
- Lisiecki, L.E., Raymo, M.E., 2005. A Pliocene-Pleistocene stack of 57 globally distributed benthic d18O records. Paleoceanography 20. https://doi.org/10.1029/2004PA001071.

- Mena, L.F., Reyes B, O., Stafford, T.W., Southon, J., 2003. Early human remains from Baño nuevo-1 cave, central patagonian Andes, Chile. Quaternary international, south America: long and winding winding roads for the first Americans at the pleistocene/holocene transition, 109–110, 113–121. https://doi.org/10.1016/S1040-6182(02)00207-0.
- Mendelová, M., Hein, A.S., Rodés, Á., Xu, S., 2020. Extensive mountain glaciation in central Patagonia during marine isotope stage 5. Quaternary Science Reviews 227. https://doi.org/10.1016/j.quascirev.2019.105996, 105996.
- Méndez, C., Nuevo Delaunay, A., Reyes, O., Ozán, I.L., Belmar, C., López, P., 2018. The initial peopling of Central Western Patagonia (southernmost South America): late Pleistocene through Holocene site context and archaeological assemblages from Cueva de la Vieja site. Quaternary International, Mobility and Use of Space in Late Pleistocene South America: Discussing Early Human Regional Trajectories 473, 261–277. https://doi.org/10.1016/j.quaint.2017.07.014.
- tories 473, 261–277. https://doi.org/10.1016/j.quaint.2017.07.014.

 Méndez, C., Nuevo-Delaunay, A., Reyes, O., Maldonado, A., García, J., 2019.

 A Systematic Strategy for Assessing the Early Surface Archaeological Record of Continental Aisén, Central Western Patagonia, pp. 34–51.

 Mercer, J.H., 1976. Glacial history of southernmost South America. Quaternary
- Mercer, J.H., 1976. Glacial history of southernmost South America. Quaternary Research 6, 125—166. https://doi.org/10.1016/0033-5894(76)90047-8.
- Miranda, C.G., 2015. Fluctuaciones glaciales en el area de Coyhaique y Balmaceda (45-46S) durante la ultima terminacion glacial: implicancias paleoecologicas y paleoclimaticas, Departamento de Ciencias Ecologicas. Universidad de Chile, Santiago.
- Moreno, P.I., Denton, G.H., Moreno, H., Lowell, T.V., Putnam, A.E., Kaplan, M.R., 2015. Radiocarbon chronology of the last glacial maximum and its termination in northwestern Patagonia. Quaternary Science Reviews 122, 233–249. https:// doi.org/10.1016/j.quascirev.2015.05.027.
- Moreno, P.I., Videla, J., Valero-Garcés, B., Alloway, B.V., Heusser, L.E., 2018. A continuous record of vegetation, fire-regime and climatic changes in north-western Patagonia spanning the last 25,000 years. Quaternary Science Reviews 198, 15–36.
- Nishiizumi, K., Imamura, M., Caffee, M.W., Southon, J.R., Finkel, R.C., McAninch, J., 2007. Absolute calibration of ¹⁰Be AMS standards. Nuclear Instruments and Methods in Physics Research Section B: Beam Interactions with Materials and Atoms 258, 403–413. https://doi.org/10.1016/j.nimb.2007.01.297.
- Parrenin, F., Masson-Delmotte, V., Köhler, P., Raynaud, D., Paillard, D., Schwander, J., Barbante, C., Landais, A., Wegner, A., Jouzel, J., 2013. Synchronous change of atmospheric CO2 and antarctic temperature during the last deglacial warming. Science 339, 1060–1063. https://doi.org/10.1126/science.1226368.
- Peltier, C., Kaplan, M.R., Birkel, S.D., Soteres, R.L., Sagredo, E.A., Aravena, J.C., Araos, J., Moreno, P.I., Schwartz, R., Schaefer, J.M., 2021. The large MIS 4 and long MIS 2 glacier maxima on the southern tip of South America. Quaternary Science Reviews 262, 106858. https://doi.org/10.1016/j.quascirev.2021.106858.
- Putkonen, J., Swanson, T., 2003. Accuracy of cosmogenic ages for moraines. Quaternary Research 59 (2), 255–261.
- Putnam, A.E., Schaefer, J.M., Barrell, D.J.A., Vandergoes, M., Denton, G.H., Kaplan, M.R., Finkel, R.C., Schwartz, R., Goehring, B.M., Kelley, S.E., 2010. In situ cosmogenic ¹⁰Be production-rate calibration from the Southern Alps, New Zealand. Quaternary Geochronology 5, 392–409. https://doi.org/10.1016/j.quageo.2009.12.001.
- Rabassa, J., Clapperton, C.M., 1990. Quaternary glaciations of the southern Andes.

 Quaternary Science Reviews 9, 153–174. https://doi.org/10.1016/0277-3791(90)
 90016-4.
- Robb, C., Willis, I., Arnold, N., Guðmundsson, S., 2015. A semi-automated method for mapping glacial geomorphology tested at Breiðamerkurjökull, Iceland. Remote Sensing of Environment 163, 80–90. https://doi.org/10.1016/j.rse.2015.03.007.
- Roe, G., 2006. In defense of Milankovitch. Geophysical Research Letters 33. https://doi.org/10.1029/2006GL027817.
- Sagredo, E.A., Moreno, P.I., Villa-Martínez, R., Kaplan, M.R., Kubik, P.W., Stern, C.R., 2011. Fluctuations of the Última Esperanza ice lobe (52°S), Chilean Patagonia, during the last glacial maximum and termination 1. Geomorphology 125, 92–108. https://doi.org/10.1016/j.geomorph.2010.09.007.
- Schaefer, J.M., Denton, G.H., Kaplan, M., Putnam, A., Finkel, R.C., Barrell, D.J.A., Andersen, B.G., Schwartz, R., Mackintosh, A., Chinn, T., Schlüchter, C., 2009. High-frequency holocene glacier fluctuations in New Zealand differ from the northern signature. Science 324, 622–625. https://doi.org/10.1126/science.1169312.
- Schaefer, J.M., Putnam, A.E., Denton, G.H., Kaplan, M.R., Birkel, S., Doughty, A.M., Kelley, S., Barrell, D.J.A., Finkel, R.C., Winckler, G., Anderson, R.F., Ninneman, U.S., Barker, S., Schwartz, R., Andersen, B.G., Schluechter, C., 2015. The southern glacial maximum 65,000 years ago and its unfinished termination. Quaternary Science Reviews 114, 52–60. https://doi.org/10.1016/j.quascirev.2015.02.009.
- Schmittner, A., Urban, N.M., Shakun, J.D., Mahowald, N.M., Clark, P.U., Bartlein, P.J., Mix, A.C., Rosell-Melé, A., 2011. Climate sensitivity estimated from temperature

- reconstructions of the last glacial maximum. Science 334, 1385–1388.
- Sigman, D.M., Haug, G.H., 2003. The biological pump in the past. Treatise on geochemistry 6, 625.
- Singer, B.S., Ackert, R.P., Guillou, H., 2004. 40Ar/39Ar and K-Ar chronology of Pleistocene glaciations in Patagonia. Geo. Society Am. Bull. 116, 434. https:// doi.org/10.1130/B25177.1.
- Smedley, R.K., Glasser, N.F., Duller, G.A.T., 2016. Luminescence dating of glacial advances at lago Buenos Aires (~46 °S), Patagonia. Quaternary Science Reviews 134, 59–73. https://doi.org/10.1016/j.quascirev.2015.12.010.
- Soteres, R.L., Peltier, C., Kaplan, M.R., Sagredo, E.A., 2020. Glacial geomorphology of the strait of magellan ice lobe, southernmost Patagonia, south America. Journal of Maps 16, 299–312. https://doi.org/10.1080/17445647.2020.1736197.
- Stern, C.R., 2004. Active Andean volcanism: its geologic and tectonic setting. Revista geológica de Chile 31, 161–206. https://doi.org/10.4067/S0716-02082004000200001.
- Stone, J.O., 2000. Air pressure and cosmogenic isotope production. J. Geophys. Res. 105, 23753–23759. https://doi.org/10.1029/2000JB900181. Strand, P.D., Schaefer, J.M., Putnam, A.E., Denton, G.H., Barrell, D.J.A., Koffman, T.N.B.,
- Strand, P.D., Schaefer, J.M., Putnam, A.E., Denton, G.H., Barrell, D.J.A., Koffman, T.N.B., Schwartz, R., 2019. Millennial-scale pulsebeat of glaciation in the southern alps of New Zealand. Quaternary Science Reviews 220, 165–177. https://doi.org/ 10.1016/j.guascirev.2019.07.022.
- Suárez, M., Demant, A., Cruz, R.D.L., Fanning, C.M., 2010. 40Ar/39Ar and U–Pb SHRIMP dating of aptian tuff cones in the aisén basin, central patagonian cordillera. Journal of South American Earth Sciences 29, 731–737. https:// doi.org/10.1016/j.isames.2009.11.003.
- Sugden, D.E., McCulloch, R.D., Bory, A.J.-M., Hein, A.S., 2009. Influence of Patagonian glaciers on Antarctic dust deposition during the last glacial period. Nature Geosci 2, 281–285. https://doi.org/10.1038/ngeo474.
- Thorndycraft, V.R., Bendle, J.M., Benito, G., Davies, B.J., Sancho, C., Palmer, A.P., Fabel, D., Medialdea, A., Martin, J.R., 2019. Glacial lake evolution and Atlantic-Pacific drainage reversals during deglaciation of the Patagonian Ice Sheet. Ouaternary Science Reviews 203, 102–127.
- Tierney, J.E., Zhu, J., King, J., Malevich, S.B., Hakim, G.J., Poulsen, C.J., 2020. Glacial cooling and climate sensitivity revisited. Nature 584, 569–573. https://doi.org/10.1038/s41586-020-2617-x.
- Tobal, J.E., Morabito, E.G., Terrizzano, C.M., Zech, R., Colavitto, B., Struck, J., Christl, M., Ghiglione, M.C., 2021. Quaternary landscape evolution of patagonia at the Chilean Triple Junction: Climate and tectonic forcings. Quaternary Science Reviews 261, 106960.
- Ton-That, T., Singer, B., Morner, N., Rabassa, J., 1999. Datacion de lavas basalticas por 40Ar/39Ar geologia glacial de la region del lago Buenos Aires, provincia de Santa Cruz, Argentina. Revisita de la Asociacion Geologica Argentina 54, 333–352
- Tulenko, J.P., Briner, J.P., Young, N.E., Schaefer, J.M., 2018. Beryllium-10 chronology of early and late wisconsinan moraines in the revelation mountains, Alaska: insights into the forcing of wisconsinan glaciation in beringia. Quaternary Science Reviews 197, 129–141. https://doi.org/10.1016/j.quascirev.2018.08.009.
- Vásquez, A., Flores-Aqueveque, V., Sagredo, E., Hevia, R., Villa-Martínez, R., Moreno, P.I., Antinao, J.L., 2022. Evolution of glacial lake cochrane during the last glacial termination, central Chilean Patagonia (~ 47 S). Front. Earth Sci 10, 817775.
- Vilanova, I., Moreno, P.I., Miranda, C.G., Villa-Martínez, R.P., 2019. The last glacial termination in the Coyhaique sector of central Patagonia. Quaternary Science Reviews 224, 105976. https://doi.org/10.1016/j.quascirev.2019.105976.
- Villa-Martínez, R., Moreno, P.I., 2021. Development and resilience of deciduous Nothofagus forests since the last glacial termination and deglaciation of the central patagonian Andes. Palaeogeography, Palaeoclimatology, Palaeoecology 574, 110459. https://doi.org/10.1016/j.palaeo.2021.110459.
- Weller, D.J., de Porras, M.E., Maldonado, A., Méndez, C., Stern, C.R., 2019. New age controls on the tephrochronology of the southernmost andean southern volcanic Zone, Chile. Quaternary Research 91 (1), 250–264.
- Wolff, E.W., Fischer, H., Fundel, F., Ruth, U., Twarloh, B., Littot, G.C., Mulvaney, R., Röthlisberger, R., de Angelis, M., Boutron, C.F., Hansson, M., Jonsell, U., Hutterli, M.A., Lambert, F., Kaufmann, P., Stauffer, B., Stocker, T.F., Steffensen, J.P., Bigler, M., Siggaard-Andersen, M.L., Udisti, R., Becagli, S., Castellano, E., Severi, M., Wagenbach, D., Barbante, C., Gabrielli, P., Gaspari, V., 2006. Southern Ocean sea-ice extent, productivity and iron flux over the past eight glacial cycles. Nature 440, 491–496. https://doi.org/10.1038/nature04614.
- Wright, H.E., Mann, D.H., Glaser, P.H., 1984. Piston corers for peat and lake sediments. Ecology 65 (2), 657–659.
- Yan, Q., Owen, L.A., Zhang, Z., Wang, H., Wei, T., Jiang, N., Zhang, R., 2021. Divergent evolution of glaciation across High-Mountain Asia during the last four glacialinterglacial cycles. Geophysical Research Letters n/a, e2021GL092411. https:// doi.org/10.1029/2021GL092411.